R.R.

Research and Development Technique for Estimating Airflow and Diffusion Parameters in Connection with the Atmospheric Water Resources Program

Final Report

August 1969

FLUID MECHANICS PROGRAM
ENGINEERING RESEARCH CENTER
COLLEGE OF ENGINEERING
COLORADO STATE UNIVERSITY
FORT COLLINS, COLORADO

Research and Development Technique for Estimating Airflow and Diffusion Parameters in Connection with the Atmospheric Water Resources Program

Final Report

August 1969

Prepared by

J. E. Cermak
L. O. Grant
M. M. Orgill

Period March 15, 1968 to June 30, 1969
Atmospheric Water Resources Research
Bureau of Reclamation
Contract No. 14-06-D-6455

Fluid Dynamics and Diffusion Laboratory
College of Engineering
Colorado State University
Fort Collins, Colorado
80521

CER69-70JEC-LOG-MMO-11

Abstract

A stably stratified atmospheric boundary layer was simulated in a wind tunnel and utilized to determine radioactive krypton dispersion patterns over a 1:9600 scale model of the Eagle River Valley and topography surrounding Climax, Colorado. Geometric, dynamic, and thermal similarity are considered, primarily, for barostromatic airflow. Similarity criteria for transport and dispersion are considered also.

This is the first time that a barostromatic airflow produced by cooling with dry ice has been documented by temperature and velocity profile measurements. Field data indicate that airflow and temperature characteristics over the model are approximately similar to a prototype storm.

Dispersion measurements were taken by using sources representative of field ground sources. Model and field measurements confirm that seeding nuclei are reaching the target area from the present existing ground sources. Limited field measurements of ice nuclei concentrations at Chalk Mountain show a variation of 5 to 300 part./liter or

$$\frac{\overline{\chi}\,\overline{U}}{Q} \sim 1 \times 10^{-9} m^{-2} \text{ to } 68 \times 10^{-9} m^{-2} .$$

Concentration values deduced from radioactive gas measurements over the model show values within the same range but closer to the optimum values indicated by present cloud physics models, i.e.,

$$\frac{\overline{\chi}\,\overline{U}}{Q} \sim 15 \text{ to } 18 \times 10^{-9} m^{-2} .$$

The barostromatic airflow model indicated that topography plays an important role in determining the downwind direction of the particulate plume.

Table of Contents

List of Figures

Nomenclature

Symbols		Dimensions
θ	Potential temperature	T
C.p.m.	Counts per minute	$\frac{\text{counts}}{t}$
Ci	Radioactive unit	curie
$\overline{\chi}$	Average concentration	ML^{-3}
Q	Source strength; time rate of material emission from a continuous source	MT^{-1}
$\overline{U}$	Mean velocity through the vertical extent of a particulate material plume	Lt^{-1}
ρ	Density of air	ML^{-3}
x,y,z	Horizontal and vertical coordinates	L
u,v,w	Horizontal and vertical velocities	Lt^{-1}
T	Temperature	T
R_d	Gas constant	$HM^{-1}T^{-1}$
C_p	Specific heat at constant pressure	$L^2t^{-2}T^{-1}$
ν	Kinematic viscosity	L^2t^{-1}
g	Acceleration of gravity	Lt^{-2}
k	Thermal conductivity	$HL^{-1}t^{-1}T^{-1}$
μ	Dynamic viscosity	$ML^{-1}t^{-1}$
Φ	Dissipation function	$ML^{-1}t^{-3}$
t	Time or sampling time	t
K_H	Exchange coefficient for heat	L^2t^{-1}
K_M	Exchange coefficient for momentum	L^2t^{-1}
$\Delta\overline{U}$	Difference of mean velocities over a arbitrary distance	Lt^{-1}

Symbols		Dimensions
$\vec{r}$	Vector distance downwind from source	L
V_s	Effluent ejection speed	Lt^{-1}
ρ_s	Mass density of effluent	ML^{-3}
Co	Depletion by coagulation	$ML^{-2}t^{-1}$
Λ	Depletion by interception with aerosols (washout, etc.)	$ML^{-2}t^{-1}$
V_{gr}	Sedimentation velocity (gravity)	Lt^{-1}
R	Depletion by chemical, radiative, and radioactive transformation	$ML^{-2}t^{-1}$
E	Depletion by electrification effects	$ML^{-2}t^{-1}$
I	Depletion by storage and reflection from land, snow and water surface	$ML^{-2}t^{-1}$
$\vec{H}$	Topographic profile (x,y,z)	L
ε	Height of surface irregularities (trees, etc.)	L
$\vec{V}$	Vector wind velocity at a given height	Lt^{-1}
β	Coefficient of stability $\frac{1}{\theta}\frac{\partial\theta}{\partial z}$	L^{-1}
$\frac{\partial\vec{V}}{\partial z}$	Directional and speed wind shear	t^{-1}
K_{ij}; K_{ii}	Coefficients of eddy diffusivity	L^2t^{-1}
k_m	Coefficient of molecular diffusivity	L^2t^{-1}
p	Pressure	$ML^{-1}T^{-2}$
σ_y, σ_z	Standard deviation of the distribution of material in a plume in the y- and z-directions	L
σ_θ, σ_ϕ	Standard deviation of lateral and vertical wind-direction distribution	degrees or radians
ψ	Stream function	L^2t^{-1}
η	Vorticity	t^{-1}

Symbols		Dimensions
θ'	Potential temperature deviation from a base state	T
$\overline{\theta}$	Potential temperature of a base state	T
Q_T	Short-wave radiation from sun and sky	$MHL^{-2}t^{-1}$
Q_R	Short-wave radiation reflected from the earth	$MHL^{-2}t^{-1}$
$Q_{L\downarrow}$	Long-wave radiation received by the surface from the atmosphere	$MHL^{-2}t^{-1}$
$Q_{L\uparrow}$	Long-wave radiation emitted by the surface	$MHL^{-2}t^{-1}$
Q_G	Transfer of heat through the ground	$MHL^{-2}t^{-1}$
Q_H	Turbulent transfer of sensible heat to the atmosphere	$MHL^{-2}t^{-1}$
Q_E	Latent heat of evaporation (condensation)	$MHL^{-2}t^{-1}$

A. Introduction

1. General statement of the problem

One of the revolutionary discoveries of cloud physics took place during 1947 when Vonnegut discovered the great efficiency of silver iodide as an ice-crystal nucleus. Since then introduction of silver iodide into cloud structures has become the major technique used in cloud modification studies.

Silver iodide acts in a cloud in essentially the same manner in which the natural freezing nuclei in the atmosphere act. It is, therefore, only necessary to distribute silver iodide smoke through the airmass in which clouds are forming in order for it to influence the cloud's microstructure.

Successful cloud seeding depends upon the introduction of sufficient artificial nuclei (e.g., silver iodide) into supercooled clouds to obtain optimum crystal concentrations. If the concentration of crystals in the cloud should be less than the optimum concentration, then not all of the vapor provided by the orographic updraft can be readily condensed upon the snow crystals. When the concentration of crystals is above the optimum number overseeding may occur and the resultant precipitation may be less than would have occurred naturally. Ludlam (1955) calculated a mean requirement of approximately 20 crystals per liter as the optimum number in orographic clouds. Grant, et al. (1968) have estimated the optimum concentration of crystals needed to insure an efficient precipitation process in the Climax, Colorado area as 5 to 100 per liter depending on the range of temperatures (-13°C to -35°C)

and vertical velocities (0.1 to 1.5 m/sec) that occur at this location.

Studies have indicated that orographic cloud systems in which systematic condensation is caused by geographical obstacles are most suitable for seeding. However, the realization of the delivery of the optimal distribution of seeding material to orographic cloud systems presents a complex theoretical and operational problem.

Several techniques such as, aircraft, ground generators, balloons, rockets, antiaircraft guns and natural rising air currents have been employed in an attempt to place the seeding material within the clouds. For storm situations in the Rocky Mountains, ground-based generators are usually used due to their continuous seeding capability, low cost, and safety features. However, aerial line sources are sometimes employed when atmospheric conditions are not too severe.

An adequate field sampling program for dispersion measurements in mountainous terrain to determine the effectiveness of ground based generators presents complex operational and logistical problems. An alternative method consists of making transport and dispersion measurements over a scale model of the terrain placed in a simulated atmospheric flow and to make a few complementary field measurements to confirm the laboratory results. This procedure appears to be basic for planning weather modification operations in new areas where information regarding local dispersion processes may not be available.

The first problem in pursuing the alternative method is to establish the validity with which wind tunnel models will simulate the dispersion phenomena. A second problem is to develop numerical models which will permit digital computers to be used for correlating laboratory and

field data and to perhaps eliminate much of the present need for both laboratory and field measurements. A study of the second problem must be reserved for a future effort.

2. General objectives of the proposed research

The following are the general objectives for the proposed research.

a. Determine the full capability for laboratory simulation of flow over mountain barriers.

b. Investigate the feasibility of simulating dispersion characteristics and transport of particulate material such as silver iodide with a wind tunnel model.

c. Continue evaluation of the use of wind tunnel simulation for weather modification operations in various types of orographic terrain.

d. Obtain field data on the relative dispersion and transport characteristics of tracers with particle sizes ranging from meter to molecular sizes.

e. Formulate a numerical model for transport and dispersion over irregular terrain.

f. Establish criteria for modeling operational programs for weather modification.

3. Summary of experimental periods

The experimental program started with the construction of the Eagle River-Climax topographic model which simulated the northwest wind direction. The scale of the model is 1:9600 and the dimensions of the

overall model is approximately 25 ft x 5 ft 10 in (Fig. 1).

Another topographic model was constructed of Elk Mountain, Wyoming at the same scale. This model will be utilized in future studies of comparing laboratory and field data. Construction details of the models were given in earlier progress reports (Cermak 1968).

Five experimental periods utilizing the Colorado State University low speed wind tunnel have been completed and a brief summary of the principal accomplishments is given in the following tabulation:

1st Experimental Period — August 27-29, 1968

Objective: To study the problem of modifying velocity profiles for the Eagle River-Climax topographic model:

a. Preliminary velocity profile data were obtained for smooth tunnel floors and over the model for different upstream conditions such as, screens, roughness, etc..

b. The mean surface airflow and deviation of surface directions from freestream direction (320°) were observed by using small pivoted vanes.

2nd Experimental Period — October 10-29, 1968

Objective: To obtain preliminary diffusion and turbulence data for the neutral airflow case and to explore the flow with a stable stratification:

a. Measurement of static pressure over model (freestream air speed ~ 12 m/s).

b. Obtained diffusion measurements over model by using helium as a tracer. Measurements were taken using a MS-12 Vecco-leak detector.

Sources: Minturn and Redcliff

Freestream Speed: 12 m/s

Results: Measurements gave a reasonable picture of the tracer plume but the helium tracer may have been too buoyant (see Interim Report February 1969).

c. Measurement of turbulence for neutral airflow. Longitudinal turbulent intensity was obtained at one location near Redcliff, a generator site.

d. Dry ice was used to produce a stable airflow over model. Smoke-wire technique was utilized to obtain velocity profiles.

3rd Experimental Period January 4-8, 1969

Objective: Further investigation of upstream conditions in order to determine which combination of screens, etc., are likely to simulate prototype conditions.

a. Velocity profiles and longitudinal turbulence data obtained for different upstream conditions.

b. Qualitative diffusion experiments using titanium tetrachloride as a tracer.

Sources: Upstream and leeward of Red and White Mountain

Freestream Airspeed: 12 m/s

Results: Pronounced separation of airflow was observed in the lee of Red and White mountain producing a definite lateral wind component in the upstream part of the Eagle River Valley. This lateral component diminishes once the flow enters the valley near Minturn. Separation acts to

strongly diffuse the chemical smoke near the entrance of the valley.

4th Experimental Period March 1-April 2, 1969

Objective: To obtain diffusion data for the Eagle River Valley-Climax model using a radioactive gas.

a. Diffusion measurements during stable flow conditions.

   Sources: Minturn and Redcliff

   Freestream Airspeed: Approx. 25-30 cm/s

   Results: Tracer plume direction depends strongly on the topography.

b. Velocity profiles for airflow with stable conditions were obtained with smoke-wire device.

c. Diffusion measurements were taken for the neutral airflow case.

   Sources: Minturn and Redcliff

   Freestream Airspeed: 15 m/s

   Results: Tracer plume diffuses very rapidly and terrain features have a much smaller effect on the direction of tracer plume once the airflow has passed over the Red and White mountain.

d. Wind velocity profiles were obtained for several locations on model for neutral airflow conditions.

5th Experimental Period May 28-June 16, 1969

Objective: Obtain reliable temperature profiles for stable airflow and turbulence data for the neutral airflow.

a. Obtained temperature profiles over the Eagle River-Climax model for the stable airflow case using dry ice.

b. Obtained longitudinal, lateral, and vertical turbulent intensities for the neutral airflow case.

B. Field Program

The basic features incorporated in the Climax weather modification experiment have been discussed by Grant, et al. (1968), Chappell (1967), Grant and Mielke (1967). Only aspects related to the dispersion problem will be reviewed in this section.

Six silver iodide generators are employed in the project. These are Colorado State University modified skyfire, needle-type ground generators. The seeding rate of the generators is about 20 grams of silver iodide per hour, producing about 10^{14} particles per gm AgI effective at -12°C and 4×10^{15} particles per gm AgI effective at -20°C.

The location of these generators with respect to the primary target is shown in Fig. 2. The azimuth and distance of each generator from the primary target is shown in Table 1.

TABLE 1
Location of seeding generators with respect to the primary target (after Chappell 1967).

Location	Azimuth and Distance from Target (degrees/nautical miles)
Minturn, Colorado	320/16
Redcliff, Colorado	316/11
South of Tennessee Pass	250/7
West of Leadville, Colorado	218/11
Aspen, Colorado	249/31
Reudi, Colorado	267/29

Since the Eagle River-Climax topographic model simulates the northwest wind direction only this aspect of the problem will be discussed.

Two generators located at Minturn and Redcliff, respectively, generate artifical nuclei which is released in an orographic airstream having a long, continuous fetch directed toward the target. Grant, et al.

(1968) indicates that the low level transport of the seeding materials are not critically affected by in-transit losses, such as, coagulation, ultraviolet radiation decay, and washout. Counts of ice crystals obtained by Bigg-Warner expansion type ice nuclei counters located on Chalk Mountain and the High Altitude Observatory (H.A.O.) have given reasonable evidence that some portion of the seeding material is reaching the Climax site (Cermak, et al. 1969). However, at times the seeding material may be diverted from the target area by unfavorable winds or atmospheric stability conditions. So far no field program has been initiated to actually determine the physical dimensions of the seeding nuclei plume generated by the Minturn and/or Redcliff sources.

Some preliminary temperature and wind soundings were taken during a field program last December in an effort to find out the characteristics of the northwest flow. These data combined with some past data have improved our understanding of the stability and wind conditions during northwest flow.

A radiosonde program at Chalk Mountain was started during the winter of 1967 and has provided vertical temperature and humidity data for many of the winter storm situations. Figure 3 shows a mean sounding during northwest flow conditions when snow was occurring in the Climax area. The temperature distribution is generally stably stratified but exhibit near neutral $(\frac{\partial \theta}{\partial z} \sim 0)$ conditions in the lower 600 meters. During single storm events such as shown in Fig. 4 neutral and inversion layers several meters thick may be embedded in the stably stratified flow.

Temperature inversions are not a rare occurrence in this region. Considering all of the 77 temperature soundings analyzed to date 35% of

these soundings exhibit some type of temperature inversion. This is an important aspect of the dispersion problem since low level temperature inversions may inhibit the vertical dispersion of particulate matter.

Some preliminary sampling of the northwest airstream has been attempted with pilot balloons during one storm situation. Pilot balloon observations were taken in the Eagle River Valley near Camp Hale and the data reduced by computer. Velocity profiles are presented in Figs. 5 and 6.

One remarkable feature is the similar alignment of the external valley wind direction with the topographic model's freestream wind direction (~320°). Generally, two general wind regimes or profiles may be distinguished,

1) an intervalley profile,

2) an external valley profile.

The intervalley profile appears characterized by a layer of small velocities and vertical wind shears which extends to the tops of the mountains (3600 to 3800 meters). Wind directions are relatively variable in this layer. The external valley profile is characterized by increased wind velocities and vertical wind shears but less variability in wind direction. Additional wind data will be necessary to determine how typical these velocity profiles are for other northwest flow situations.

C. Laboratory Study

1. Airflow types

Two general types of airflow were generated in the wind tunnel for this study--1) neutral airflow, where static stability is assumed neutral and the pressure field is determined by the geometry of the terrain features. If the terrain features are sharp, the flow patterns are not influenced by viscous forces and Reynold's number differences between the model and prototype. Irreversibility in the flow is usually due to the production of separation eddies, which appear on the lee side of obstacles. 2) Barostromatic* airflow, where the air is stably stratified due to density or temperature stratification. This type of airflow is generally quasi-laminar and with proper density stratification gravity waves and hydraulic "jumps" occur. Large vertical temperature gradients and low flow velocities are required in order to produce this type of flow in the wind tunnel.

Most topographic model studies have been made with neutral flow while barostromatic airflow has just recently been investigated in the wind tunnel. However, an effort was made in 1941 by Abe to study flow over Mt. Fuji with an air stream stratified by solid carbon dioxide. Table 2 gives a listing of terrain models which have been studied and the type of flow used.

An exploratory set of dispersion measurements was conducted during the 2nd experimental period using a neutral flow and these results were presented in our Interim Report, February 1969. Since helium was utilized

---

* Word derived from Greek and adopted by R. S. Scorer (1953).

TABLE 2

Laboratory Model Studies of Airflow over Irregular Terrain

Author	Topographic Site	Problems	Type of Airflow
Garrison & Cermak 1968	San Bruno Mountain, California	Topographic effects on airflow	Neutral and Barostromatic (dry ice)
Hsi, Binder & Cermak 1968	Green River, Utah	Topographic effects on airflow	Neutral
Lin & Binder 1967	Idealized Hill's	Mountain lee waves	Barostromatic
Meroney & Cermak 1967	San Nicolas Island, Calif.	Topographic effects and diffusion	Neutral and Barostromatic
Cermak & Peterka 1966	Point Arguello, California	Topographic effects and diffusion	Barostromatic
Chang 1966	Idealized Hill	Wake effects	Neutral
Plate & Lin 1965	Idealized Hill's	Velocity profiles & wake pattern	Neutral
Halitsky, Magony & Halpern 1964-65	Mountains near Manchester, Vermont	Topographic effects on airflow	Neutral
Briggs 1963	Rock of Gibraltar	Turbulence patterns	Neutral
Halitsky, Tolciss, Kaplin, & Magony 1962-63	Bear Mountain, New York	Turbulence & wake pattern	Neutral
Nemoto 1961	Enoshima & Akashi-channel, Japan	Turbulence & velocity profiles	Neutral
Long 1959	Sierra Nevada Mountains, Calif.	Mountain lee waves	Barostromatic (brine solution)
Suzuki & Yabuki 1956	Idealized Hill's	Mountain lee waves	Barostromatic (brine solution)
Abe 1941	Mt. Fuji, Japan	Mountain clouds & topographic effects	Barostromatic (dry ice)
Field & Warden 1929-30	Rock of Gibraltar	Topographic effects & turbulence	Neutral

as a tracer the dispersion results were subject to possible buoyancy effects. The neutral stability flow was repeated during the 4th experimental period using neutrally buoyant radioactive krypton as a tracer. Although these data are not completely analyzed the qualitative aspects of the tracer plume and dispersion are similar to the results obtained with the helium tracer. A detailed summary of this case will appear in a dissertation by Orgill.

The radioactive krypton method for dispersion measurements gave further impetus to studies with barostromatic airflow. This type of flow is preferable because of the realism provided by the temperature stratification. Since the actual atmosphere is usually stably stratified, the barostromatic model tends to improve the similarity.

2. Experimental procedure

a. Wind tunnel

All the experimental work was accomplished in the Colorado State University low-speed recirculation wind tunnel. The tunnel is driven by a 75 h.p. DC motor and contains a 9.2 meter test section length which is 1.8 x 1.8 meters in cross section. A complete description of the wind tunnel is given in a brochure-Fluid Mechanics Program (1966).

The experimental arrangement in the tunnel for the barostromatic airflow case is shown in Fig. 7. To produce a temperature stratification in the tunnel 600 lbs of dry ice was located on the floor of the upstream section of the tunnel. A board 70 x 47 in blocked the upstream section forcing the cold air to flow across the topographic model. The dry ice produced an airflow which reversed direction with height, therefore, in

order to eliminate this undersirable feature the wind tunnel was set at a very low speed setting so that just enough warm air would move over the cold air to eliminate the backflow. This arrangement also improved the velocity profile similarity.

In order to utilize the radioactive tracer an exhaust fan was mounted on the top of the west section of the tunnel where conduit sections extended to an outside window. Such an arrangement assured keeping the radioactive background count in the wind tunnel at very safe working levels.

b. Velocity profiles

The mean velocity distributions over the model were measured by means of the smoke wire probe (Fig. 8). A nichrome wire 3.81×10^{-3} cm in diameter and 30 cm (variable) in length is coated with low viscosity oil which is vaporized by passage of an electrical pulse through the wire. The resultant line source of smoke is then photographed. The distance traveled by a point in the smoke trace downwind from the vertical wire is proportional to the local mean wind speed. Figure 9 shows the smoke wire system as utilized during velocity profile experiments. A remote oiler system (not shown) provided a means of coating the wire without frequently disturbing the airflow in the tunnel.

Figure 10 shows a photograph of a typical smoke line obtained from the smoke wire system. A serious problem develops upon using dry ice since a dense cloud of water vapor forms in the tunnel which often obscures the smoke line in the lower levels. Although, the problem can be alleviated in the future it reduced the quality of data during this experimental period.

The pictures of the smoke lines were viewed by a STK-1 stereo-comparator and the pertinent data were digitized on punch cards. A simple computer program obtained plots of velocity vs height. Figure 11 shows three velocity profiles taken at the Pando location on the model corresponding to the field location. Heights have been converted to the prototype scale.

Velocity profile data as derived from the smoke wire system are essentially one component of the total velocity vector, i.e., the component along the wind tunnel axis. Since the flow over the topographic model is three dimensional the smoke wire measurements underestimate the total velocity vector. An attempt will be made to obtain at least two-dimensional velocities in future experiments.

The reproducibility of the velocity profiles at one location is illustrated in Fig. 11. Calculation of a coefficient of variation at selected elevations indicated a variation in velocity between 5 and 25%. Variations of the velocity profiles may be due to unsteadiness in the flow and errors in measurement. Detailed error analysis of the smoke wire system will be presented later by Orgill (dissertation).

c. Temperature measurements

Temperature profiles over the model were obtained using a copper-constantan thermocouple attached to a vertical and horizontal traversing carriage. Figure 12 shows the experimental arrangement in the tunnel.

Since the thermocouple had a relatively slow response time it was positioned at a location and left there until the temperature

reading became stabilized; a reading was made, and the probe was repositioned. Plots of temperature were obtained with an X-Y plotter.

Vertical temperature profiles were obtained for nine different locations on the topographic model. Figure 13 shows the temperature field as deduced from these measurements. Temperature measurements were within ±2°C.

d. Dispersion measurements

Concentration measurements over the topographic model was obtained by releasing radioactive krypton continuously from ground level sources and using Geiger-Mueller tubes to determine the relative amount of krypton in samples of the gas-air mixture. The method was originally developed by Chaudhry (1969). The experimental equipment is shown in Fig. 7.

Once the flow in the tunnel was stabilized* a mixture of Kr-85 and air was released from a source within the tunnel (Fig. 14). In order to minimize buoyant effects due to the cold tunnel air, two sets of cooling coils were placed between the gas source and the source opening in the tunnel. The flow rate of Kr-85 mixture was controlled by a pressure regulator at the bottle outlet and monitored by a flow meter. Source concentration was 1.17 μ-curie/cc of Kr-85, a beta emitter (half life-10.3 years).

A sampling rake of eight probes (Fig. 14) was mounted on a traversing carriage whose horizontal and vertical positions were controlled

---

* The smoke wire system was used to assure that air flow was stabilized and that backflow was not present, (not shown in Fig. 7).

remotely from outside the tunnel. The inner diameter of the sampling probes was 0.4 cm. Samples were aspirated at a constant rate of 200 cc/min into eight TGC-308 Tracerlab Geiger-Mueller sidewall cylindrical counters. Samples were flushed through the counting tubes for at least 5 minutes after which each sample was subsequently counted for 2 and sometimes 3 minutes on a Nuclear Chicago Ultra-scaler Model 192A. Background samples of the radiation were taken several times during an experiment.

Two separate source locations were used--, simulation of a Minturn source and a Redcliff source. Vertical and lateral profiles were made 7.0, 13.8, 22.5, and 30 km downwind from the Minturn source and 3.5, 12.5, and 19.2 km downwind from the Redcliff source. The limited number of profiles depended on the duration of the dry ice which was effective for 6 to 8 hours.

The procedure for analyzing the dispersion data is as follows: Counts of the pulses generated in the G.M. tubes were recorded for all eight probes at the various locations. These counts were transformed into concentration values, by the following steps:

$$\text{Cpm-Background (Cpm)} = \text{Cpm}^*$$

$$\text{Cpm}^* \times \text{counting yield } (\mu\mu\text{Ci/cc/Cpm}) = \overline{\chi}(\mu\mu\text{Ci/cc}).$$

The counting yield varies according to the G.M. tube as shown below.

G.M. Tube	1	2	3	4	5	6	7	8	
Counting yield	1.16	1.43	1.16	1.16	1.22	1.25	1.2	1.2	(μμCi/cc/Cpm).

For counts over 1,000 a deadtime correction* has to be applied to the

* The time taken for the positive space charge to move sufficiently far from the anode for further pulses to occur (Faires and Parks, 1960).

readings, in this case, the correction is,

$$\text{Cpm-Background} = \text{Cpm}^*$$

$$\frac{\text{Cpm}^*}{1 - 1.77 \times 10^{-6} \times \text{Cpm}^*} = \text{Cpm}^{**}$$

$$\text{Cpm}^{**} \times \text{Counting yield} = \overline{\chi}(\mu\mu\text{Ci/cc}).$$

Concentration values $\overline{\chi}$ were determined for the known probe heights and then plotted against height. Concentration curves were drawn for each location where measurements were taken on the model and then values of $\overline{\chi}$ were interpolated for every 100 meters of prototype scale. The quanity $\overline{\chi}\,\overline{U}/Q$ was then computed for every 100 meters. A sample computation is shown below,

$q = 350$ cc/min $= 5.84$ cc/sec

$Q = 1.17\ \mu$Ci/cc $\times$ 5.84 cc/sec $= 6.84\ \mu$Ci/sec

let $\overline{\chi} = 1800\ \mu\mu\text{Ci/cm}^3$

$\overline{U} = 12$ cm/sec

then

$$\frac{\overline{\chi}\,\overline{U}}{Q} = \frac{1800 \times 12}{6.84} = \frac{3158 \times 10^{-6}}{\text{cm}^2} = \frac{3158 \times 10^{-2}}{\text{m}^2} \quad .$$

Since these values apply to the model we need to scale the concentration parameter to the prototype. If we write,

$$\frac{\overline{\chi}_m\,\overline{U}_m\sigma_{y_m}\sigma_{z_m}}{Q_m} = \frac{\overline{\chi}_p\overline{U}_p\sigma_{y_p}\sigma_{z_p}}{Q_p} \qquad (1)$$

and with rearrangement

$$\frac{\overline{\chi}_m\overline{U}_m\sigma_{y_m}\sigma_{z_m}}{Q_m\sigma_{y_p}\sigma_{z_p}} = \frac{\overline{\chi}_p\overline{U}_p}{Q_p} = \left(\frac{\overline{\chi}\,\overline{U}}{Q}\right)_{\text{prototype}} \qquad (2)$$

then its possible to accomplish this goal if σ_z and σ_y for model and prototype can be evaluated. Various forms for σ_z and σ_y have been derived and are expressed in Table 3.

TABLE 3

Summary of Diffusion Coefficients

Identification	Diffusion coefficients	Plume dimensions
Sutton	C_y, C_z, n_y, n_z	$\sigma_y = \frac{1}{2^{\frac{1}{2}}} C_y x^{2-n_y/2}$
		$\sigma_z = \frac{1}{2^{\frac{1}{2}}} C_z x^{2-n_z/2}$
Fickian	K_x, K_y, K_z	$\sigma_y = (2K_y t)^{\frac{1}{2}}$
		$\sigma_z = (2K_z t)^{\frac{1}{2}}$
Cramer	$\sigma_\theta, \sigma_\phi, p, q$	$\sigma_y = \sigma_\theta x^p$
		$\sigma_z = \sigma_\phi x^q$
Pasquill*	$\sigma_{\theta(T,t)}, \sigma_{\phi(T,t)}$	$\sigma_y = \sigma_{\theta(T,t)} x$
		$\sigma_z = \sigma_{\phi(T,t)} x$

* The symbols T and t represent the sampling time and averaging time, respectively.

If σ_z and σ_y for model and prototype were avaliable by direct measurement then the result would be simple but since this is not the case and alternative procedure is selecting expressions from Table 3. The most convenient selection is Pasquill's expressions for σ_y and σ_z, then equation (2) becomes,

$$\frac{\bar{\chi}_m \bar{U}_m}{Q_m} \frac{\sigma_{\theta_m} \sigma_{\phi_m}}{\sigma_{\theta_p} \sigma_{\phi_p}} \frac{x_m^2}{x_p} = \left(\frac{\bar{\chi}\,\bar{U}}{Q}\right)_{\text{prototype}} . \tag{3}$$

The choice is somewhat arbitrary because measurements of the various independent variables in the σ_z and σ_y expressions are not available. One recourse is to assume that

$$\frac{\sigma_{\theta_m}\sigma_{\phi_m}}{\sigma_{\theta_p}\sigma_{\phi_p}} = 1 \qquad (4)$$

inferring that the standard deviations of the lateral and vertical wind direction distribution are similar for model and prototype. Then using the scaling factor 1:9600 the prototype concentration parameter can be computed by,

$$\left(\frac{\bar{\chi}\,\bar{U}}{Q}\right)_{\text{model}} \frac{1}{(9600)^2} = \left(\frac{\bar{\chi}\,\bar{U}}{Q}\right)_{\text{prototype}} . \qquad (5)$$

This simple scaling of the concentration parameter from model to prototype appears to give comparable results as indicated on page 33.

3. Similarity criteria

a. Assumptions and basic equations

In order that the flow in any laboratory model should be of value in interpreting or predicting the observed flow in the atmosphere, it is essential that the two systems should be dynamically, thermally, and geometrically similar. This means that it must be possible to describe the flow in the two systems by the same equations after appropriate adjustment of the units of length, time, etc. has been made.

Several difficulties arise in attempting to devise a model which will be similar to the atmosphere. The difficulties are principally due to the limitations of the laboratory apparatus in reproducing a

scaled down model atmosphere. These problems require a simplification of the basic equations of the atmosphere by a set of restrictive assumptions. The principal assumptions are:

1) In the case of the barostromatic airflow experiment the flow was considered quasi-laminar and therefore the turbulent terms in the equation of motion are neglected.

2) The prototype region is comparatively small (largest length dimension is less than 50 miles) so the Coriolis acceleration terms in the equation of motion are considered negligible compared to effects of the convective accelerations due to irregular terrain.

3) Since the vertical variation of the hydrostatic pressure in the atmosphere can not be simulated the model airflow is considered incompressible, i.e.,

$$\frac{1}{\rho}\frac{D\rho}{Dt} = -\left(\frac{\partial u}{\partial x} + \frac{\partial v}{\partial y} + \frac{\partial w}{\partial z}\right) = 0 \ . \tag{6}$$

One consequence of this restriction can be obtained by taking the logarithmic derivative of the Poisson's equation

$$\theta = T\left(\frac{1000}{\rho}\right)^{\frac{R_d}{C_p}} \tag{7}$$

with respect to z ,

$$\frac{1}{\theta}\frac{d\theta}{dz} = \frac{1}{T}\frac{dT}{dz} - \frac{R_d}{C_p}\frac{1}{p}\frac{dp}{dz} \tag{8}$$

since dp/dz for the model flow is assumed negligible

$$\frac{1}{\theta}\frac{d\theta}{dz} = \frac{1}{T}\frac{dT}{dz} \tag{9}$$

which shows that for incompressible flow the temperature is equivalent to the potential temperature.

4) Wind velocity vector is assumed steady, i.e., $\frac{\partial u}{\partial t}$, etc. = 0 and in addition, no directional wind shear is assumed due to the thermal wind or horizontal temperature gradients. However, unsteadiness in the flow and directional wind shear could occur due to the irregular terrain.

5) Gravity force is approximately the same for model and prototype.

6) Effects of condensation, evaporation, convection and radiation are negligible.

With these assumptions the basic equations for the model airflow can be written as follows:

Equation of motions

$$u\frac{\partial u}{\partial x} + v\frac{\partial u}{\partial y} + w\frac{\partial u}{\partial z} = -\frac{1}{\rho}\frac{\partial p}{\partial x} + \nu[\frac{\partial^2 u}{\partial x^2} + \frac{\partial^2 u}{\partial y^2} + \frac{\partial^2 u}{\partial z^2}]$$

$$u\frac{\partial v}{\partial x} + v\frac{\partial v}{\partial y} + w\frac{\partial v}{\partial z} = -\frac{1}{\rho}\frac{\partial p}{\partial y} + \nu[\frac{\partial^2 v}{\partial x^2} + \frac{\partial^2 v}{\partial y^2} + \frac{\partial^2 v}{\partial z^2}] \qquad (10)$$

$$u\frac{\partial w}{\partial x} + v\frac{\partial w}{\partial y} + w\frac{\partial w}{\partial z} = -g + \nu[\frac{\partial^2 w}{\partial x^2} + \frac{\partial^2 w}{\partial y^2} + \frac{\partial^2 w}{\partial z^2}] \quad .$$

Continuity equation

$$\frac{\partial u}{\partial x} + \frac{\partial v}{\partial y} + \frac{\partial w}{\partial z} = 0 \quad . \qquad (11)$$

Poisson's equation

$$\frac{1}{\theta}\frac{d\theta}{dz} = \frac{1}{T}\frac{dT}{dz} \quad . \qquad (12)$$

Equation of heat transfer

$$\rho Cp(\frac{\partial T}{\partial t} + u_j \frac{\partial T}{\partial x_j}) = \frac{\partial}{\partial x_j}(k\frac{\partial T}{\partial x_j}) + \Phi \qquad (13)$$

where

$$\Phi = \mu\{2[(\frac{\partial u}{\partial x})^2 + (\frac{\partial v}{\partial y})^2 + (\frac{\partial w}{\partial z})^2] + (\frac{\partial v}{\partial x} + \frac{\partial u}{\partial y})^2 + (\frac{\partial w}{\partial x} + \frac{\partial u}{\partial z})^2 + (\frac{\partial w}{\partial y} + \frac{\partial v}{\partial z})^2\} \quad . \tag{14}$$

b. Geometric similarity

Irregular terrain is difficult to classify but nevertheless generally three types can be recognized; 1) Blocking ridge or mountain range, where the obstacle acts to impede or block the airflow. The only avenue for the oncoming airflow is to ascend the blocking topography. 2) Valley, where the oncoming airflow may be channeled by the surrounding walls of the valley. 3) Singular mountain, where a substantial portion of the oncoming airflow is forced to diverge and flow around the obstacle instead of over it.

The terrain of the Eagle River Valley and Climax area has characteristics of three types, blocking ridge (Red and White Mountain), valley (Eagle River Valley and others) and singular mountain (Chicago Ridge and Chalk Mountain).

Geometric similarity was achieved by a 1:9600 scale topographic model as discussed in section A.3.

c. Dynamical and thermal similarity

Strict dynamical and thermal similarity as required by identity of the equations of motion and heat transfer for the two systems is virtually impossible. Therfore, at the outset one must be prepared to relax the requirement for complete similarity and attempt to achieve the best approximation.

To find the relevant scaling parameters for dynamical and thermal similarity the dependent and independent variables for the various equations may be expressed in dimensionless form using the following scaling quantities:

$$x_i' = \frac{x_i}{L^*} \;,\; u_i' = \frac{u_i}{U^*} \;,\; p' = \frac{p}{\Delta p^*} \;,\; \rho' = \frac{\rho}{\rho^*} \;,\; g' = \frac{g}{g^*} \;,\; \mu' = \frac{\mu}{\mu^*}$$

$$k' = \frac{k}{k^*} \;,\; t' = t\frac{U^*}{L^*} \;,\; T'\frac{T}{\Delta T^*} \;,\; C' = \frac{c_p}{c_p^*} \quad . \tag{15}$$

In terms of the new dimensionless quantities the vertical equation of motion assumes the form,

$$u'\frac{\partial w'}{\partial x'} + v'\frac{\partial w'}{\partial y'} + w'\frac{\partial w'}{\partial z'} = g'\frac{1}{Fr} + \nu'\frac{1}{Re}\left[\frac{\partial^2 w'}{\partial x'^2} + \frac{\partial^2 w'}{\partial y'^2} + \frac{\partial^2 w'}{\partial z'^2}\right] \tag{16}$$

and one of the horizontal equations of motion say x - component is,

$$u'\frac{\partial u'}{\partial x'} + v'\frac{\partial u'}{\partial y'} + w'\frac{\partial u'}{\partial z'} = -\,Eu\frac{1}{\rho'}\frac{\partial p'}{\partial x'} + \nu'\frac{1}{Re}\left[\frac{\partial^2 u'}{\partial x'^2} + \frac{\partial^2 u'}{\partial y'^2} + \frac{\partial^2 u'}{\partial z'^2}\right] \tag{17}$$

and the equation of heat transfer,

$$\rho' C_p'\left(\frac{\partial T'}{\partial t'} + u'\frac{\partial T'}{\partial x'} + v'\frac{\partial T'}{\partial y'} + w'\frac{\partial T'}{\partial z'}\right) = \frac{1}{Pr}\frac{1}{Re}\left\{k\left(\frac{\partial^2 T'}{\partial x'^2} + \frac{\partial^2 T'}{\partial y'^2} + \frac{\partial^2 T'}{\partial z'^2}\right)\right\}$$

$$+ Ek\,\frac{\Phi'}{Re} \quad . \tag{18}$$

Where

$$\text{Re (Reynolds number)} = \frac{U^*L^*}{\nu^*}$$

$$\text{Fr (Froude number)} = \frac{U^{*2}}{L^*g^*}$$

$$\text{Eu (Euler number)} = \frac{\Delta P^*}{\rho^* U^{*2}}$$

$$\text{Pr (Prandtl number)} = \frac{\mu^* Cp^*}{k^*}$$

$$\text{Ek (Eckert number)} = \frac{U^{*2}}{Cp^*\Delta T^*}$$

would have to be the same for model and prototype.

Reynolds number similarity

Reynolds number equality for prototype and model is not possible unless one assumes that the model molecular kinematic viscosity is equivalent to an average prototype eddy viscosity as done by Abe (1941) and Cermak and Peterka (1966). In this case, a comparison of the Reynolds numbers $(Re)_m$ and $(Re)_p$ may be made for estimating the degree of similarity. The ratio of these two Reynolds numbers,

$$\frac{(Re_p)_{turb}}{Re_m} = \left(\frac{U^*_p}{U^*_m}\right)\left(\frac{L^*_p}{L^*_m}\right)\frac{\nu^*_m}{(K_m)_p} \tag{19}$$

can be estimated by selecting typical values for the various ratios.

Field	Model
L* 200 meters (2×10^5cm)	20.8 cm
U* 18 m/s	18 cm/sec
$(K_M)_p \sim 10^5 cm^2/sec$	$\nu^*_m \sim 0.168\ cm^2/sec$.

Computation shows a favorable value for the Reynolds number ratio,

$$\frac{(Re_p)_{turb}}{Re_m} = 1.6 \quad .$$

Prandtl number similarity

The ratio of the two Prandtl numbers,

$$\frac{Pr_p}{Pr_m} = \left(\frac{k^*_m}{k^*_p}\right)\left(\frac{\mu^*_p}{\mu^*_m}\right)\frac{(c^*)_p}{(c^*)_m} \tag{20}$$

can be estimated in a similar manner using the following values,

Field	Model
$\overline{\mu^*}$ 1.577 g $cm^{-1}s^{-1}$	1.768 g $cm^{-1}s^{-1}$
$\overline{k^*}$ 5.365 cal $cm^{-1}s^{-1}{}^{o}C^{-1}$	6.01 cal $cm^{-1}s^{-1}{}^{o}C^{-1}$
c^*_p 0.240 cal $g^{-1}{}^{o}K^{-1}$	0.240 cal $g^{-1}{}^{o}K^{-1}$.

Computation shows a very favorable value for the Prandtl number ratio,

$$\frac{Pr_p}{Pr_m} \sim 1 \ .$$

Eckert number similarity

Similar calculations for the Eckert number show,

$$\frac{(Ek)_p}{(Ek)_m} = 1.55 \times 10^4 \ .$$

Since the Ekert number is equivalent to the Mach number, similarity is not possible because of the low model airflow speeds. One would expect that Eckert number nonsimilarity would have a small effect on the dispersion problem especially in incompressible flow.

Euler number similarity

The ratio of the two Euler numbers,

$$\frac{(Eu)_p}{(Eu)_m} = \left(\frac{\Delta P^*_p}{\Delta P^*_m}\right)\left(\frac{\rho^*_m}{\rho^*_p}\right)\frac{U^{*2}_m}{U^{*2}_p} \qquad (21)$$

show that typical values can be assigned except for ΔP^*_p and ΔP^*_m which have not been measured. The Euler number would not appear explicitly in the similarity criteria if the pressure was scaled in the following manner,

$$p' = \frac{P}{\rho^* U^{*2}} \ . \qquad (22)$$

However, if the pressure is not scaled this way then it has been assumed that geometric similarity is a sufficient condition for Euler number similarity (Cermak, et al. 1966). This assumption has not been investigated for barostromatic airflows.

For the transport and dispersion problem in the Eagle River Valley and Climax area, Euler number similarity could be important especially in the lower 500 meters of the valley. Perhaps rough estimates of ΔP_p^* and ΔP_m^* could be calculated from the equations of motion or Bernoulli's equation once adequate wind velocity profile data is available both in the field and wind tunnel.

Froude or Richardson number similarity

For the barostromatic airflow Froude number similarity is very important. Meteorologists usually utilize a related dimensionless parameter the Richardson number,

$$Ri = \frac{K_H}{K_M} \frac{g}{\theta} \frac{\frac{\partial \theta}{\partial z}}{(\frac{\partial u}{\partial z})^2} \quad .$$

Batchelor (1953) suggests that the equality of the Richardson number may be a sufficient condition for dynamic similarity for frictionless flow systems of low-speed motions.

In the expression for the Richardson number the ratio $\frac{K_H}{K_M}$ depends on stability, whereby K_H may exceed K_M in unstable air, and vice versa for stable air. Laboratory measurements suggest values close to 1 for this ratio.

Reiter and Lester (1967) have shown a strong dependence of Ri on layer thickness L . They have found a relationship,

$$Ri \propto L^p \tag{23}$$

where $0 \leq p \leq L^{4/3}$. This relationship appears to vary from case to case.

In order to check Richardson number equality for model and prototype a bulk Richardson number,

$$Ri = \frac{g}{\overline{\theta}} \frac{\Delta\theta}{(\Delta\overline{U})^2} \Delta z \qquad (24)$$

was calculated for 200 meter layer thicknesses with the ratio $\frac{K_H}{K_M}$ assumed equal to 1 . Temperature and vertical wind shears for the prototype were obtained from the 1826MST and 1639MST Pando soundings (Fig. 4 and 6). Model data were obtained from Fig. 11 and Fig. 13.

Table 4 shows these results as well as the Bulk Richardson number for a layer thickness of 2000 meters. Generally, the overall model airflow was more stable than the prototype storm. Exact similitude cannot be expected in all layers but the model Richardson numbers as compared to the prototype Richardson numbers indicate that approximate thermal and wind shear similitude is possible.

d. Similarity requirements for transport and dispersion

The average concentration $\overline{\chi}$ at a particular location in a particulate plume over mountainous terrain is affected by numerous variables, e.g., $\overline{\chi}(\vec{r}) = f(Q, V_s, \rho_s, Co, \Omega, V_{gr}, R, E, I, \vec{H}, \varepsilon, \vec{V}, \beta, \frac{\partial \vec{V}}{\partial z}, K_{ij}, t)$. Q, V_s, ρ_s are parameters depending on the source characteristics. Co, Ω, V_{gr}, R, E, I are physical variables depleting the particulate material in transit. $\vec{H}$ and ε describe the topographic terrain. $\vec{V}$ represent the transport by mean motions (synoptic, mesoscale, etc.). β, $\frac{\partial \vec{V}}{\partial z}$, K_{ij}, are parameters which influence turbulent mixing.

For a wind-tunnel model of our scale length it is very difficult to scale or simulate all aspects of the source characteristics and

TABLE 4

Bulk Richardson number for model and prototype

$$Ri = \frac{g}{\bar{\theta}} \frac{\Delta\theta}{(\Delta\bar{U})^2} \Delta z$$

Δz(meters)	Model Ri	Prototype* Ri (one storm
0-200	-0.14	0
200-400	3.4	114.3
400-600	8.8	63.9
600-800	1.3	2.1
800-1000	1.6	1.1
1000-1200	22.1	0.8
1200-1400	41.1	11.1
1400-1600	11.6	26.6
1600-1800	6.9	1.6
1800-2000	7.2	1.1
2000-2200	20.9	979
0-2000	13.7	3.8

* For the prototype, $\Delta\bar{U}$ was computed as the difference between resultant wind velocities while for the model $\Delta\bar{U}$ was computed as the difference between wind speeds along the wind tunnel axis. The model wind speeds are essentially one component of the velocity vector and underestimates the actual velocity.

variables depleting the particulate material in transit. It is likely that source characteristics are soon lost as mixing takes place downstream and exact simulation is not essential. In case of the depletion variables some like V_{gr} may be neglected since the sedimentation velocity of silver iodide particles is very small. Grant, et al. (1968) have indicated that Ω (washout), R (ultraviolet deactivation), and Co (coagulation) are not effecting low level transport of seeding materials in the Eagle River Valley and Climax area to a critical extent. Little is known in the field concerning E (electrification effects) and I (storage and reflection), therefore, these variables as well as Ω, R and Co are neglected.

The functional relation can now be written as,

$$\overline{\chi}(\vec{r}) = f(\vec{H}, \varepsilon, \vec{V}, \beta, \frac{\partial \vec{V}}{\partial z}, K_{ij}, t) \ . \tag{26}$$

The first six variables have appeared in geometric, dynamic, and thermal similarity and nothing is new except t the sampling time.

It is important to note how the time-scales differ for model and prototype. If the time-scale of the model is t_m and that of the real flow t_p, then we have,

$$t_m = \frac{L_m}{L_p} \frac{U_p}{U_m} t_p \ . \tag{27}$$

According to this relationship the critical factors governing the time-scale of the model is the geometric scale ratio and the velocity ratio. A large velocity ratio is most favorable for achieving time similarity.

If t_p = 1 hour, U_p = 22 m/s, U_m = 18 cm/s and using the present scale ratio 1:9600 then equation (27) gives t_m = 44 sec. A

typical seeding operation in the field is for 24 hours of 17.6 min model time. During our model dispersion experiments sampling time was 5 minutes or 6.8 hours field time. Thus, the sampling time for the model was rather large as compared with most field sampling times. A more favorable time similarity may be achieved by decreasing the sampling time in the dispersion experiments or achieving a larger velocity ratio for equation(27).

In cases where the surface over which the flow occurs is irregular, composed of hills and valleys, transport of a particulate material in the atmosphere may be influenced primarily by strong spatial variation in convective transport by the mean motion. This may be the case during strong stable thermal stratification. If one examines the turbulent diffusion equation;

$$\frac{\partial \bar{\chi}}{\partial t} + \bar{u}\frac{\partial \bar{\chi}}{\partial x} + \bar{v}\frac{\partial \bar{\chi}}{\partial y} + \bar{w}\frac{\partial \bar{\chi}}{\partial z} = \frac{\partial}{\partial x_i}\left(K_{ii}\frac{\partial \bar{\chi}}{\partial x_i}\right) + k_m\left[\frac{\partial^2 \bar{\chi}}{\partial x_i^2}\right] \qquad (28)$$

where

$\bar{u}_i \frac{\partial \bar{\chi}}{\partial x_i}$ --- convective transport by mean flow

$\frac{\partial}{\partial x_i}\left(K_{ii}\frac{\partial \bar{\chi}}{\partial x_i}\right)$ --- turbulent diffusion

$k_m\left(\frac{\partial^2 \bar{\chi}}{\partial x_i^2}\right)$ --- molecular diffusion

then for this type of flow system when the mean flow is assumed steady and the primary transport mechanism is the convective transport by mean motion we find,

$$\bar{u}\frac{\partial \bar{\chi}}{\partial x} + \bar{v}\frac{\partial \bar{\chi}}{\partial y} + \bar{w}\frac{\partial \bar{\chi}}{\partial z} = 0 \quad . \qquad (29)$$

4. Experimental results

a. Dispersion results

Lateral and vertical cross sections of the concentration parameter $\frac{\overline{\chi}\,\overline{U}}{Q}$ are presented in Figs. 15 and 16 for a Redcliff source. Figure 17 shows selected lateral cross sections of the same parameter for a Minturn source. High concentration values appear near valley floors and decrease with height for both sources.

The lateral cross section of the concentration parameter nearest the Minturn source which was approximately over Gilman (not shown) showed maximum concentrations somewhat elevated from the ground. We are not certain whether this is caused by topographic effects or due to possible buoyancy effects of the radioactive gas. The radioactive gas was cooled before entering the wind tunnel but we did not have a proper instrumental arrangement for measuring the source gas temperature, therefore, we have no quantitative verification on possible buoyancy effects. The concentration data for the Redcliff source showed no elevated maximum concentrations.

The preceding figures indicate that with the barostromatic air flow generated by dry ice, valley topography has a definite effect on the direction of the tracer plume. A plot of the surface concentration downstream from the Redcliff source (Fig. 18) shows the axis of peak concentration west of Chicago Ridge some 8 km from Chalk Mountain. Lateral cross sections suggest secondary maxima between Chicago Ridge and Chalk Mountain.

The topography dominated plume in the case of stable airflow

appears to be verified further by comparing this case with dispersion measurements obtained from a turbulent airflow with neutral stability as shown in Fig. 19. In this case the particulate plume appears to be less dominated by topography and as a result the peak concentration axis is observed within 2 km from Chalk Mountain.

Field measurements of ice nuclei concentrations at Chalk Mountain and optimum concentrations provides a means for checking whether the model concentration results are within an order of magnitude of field results.

For the model, the variation of $\overline{\chi}$ from Minturn and Redcliff sources at the surface near or on Chalk Mountain varies from,

$$\text{Redcliff source } \overline{\chi} \sim 30 \text{ to } 42 \text{ } \mu\mu\text{Ci/cc}^*$$

$$\text{Minturn source } \overline{\chi} \sim 144 \text{ to } 124 \text{ } \mu\mu\text{Ci/cc} .$$

If we assume that concentration values from the two sources are additive,

$$\overline{\chi}_T \sim 154 \text{ to } 186 \text{ } \mu\mu\text{Ci/cc} .$$

If the sources are also additive then

$$Q_T \sim 13.68 \text{ } \mu\text{Ci/sec} ,$$

and if $\overline{U} \sim 12$ cm/sec, then

$$\frac{\overline{\chi}\,\overline{U}}{Q_T} \sim 15 \times 10^{-9} m^{-2} \text{ to } 18 \times 10^{-9} m^{-2}$$

after scaling this parameter to the prototype.

For a silver iodide generator in the field,

---

* This variation has been computed only on the basis of the accuracy of counts due to the Geiger-Mueller tubes which is:

$$\text{counts variation} = \text{counts} \pm \sqrt{\text{counts}} \quad \text{or C.p.m.} = \frac{\text{counts}}{t(\text{min})} \pm \frac{\sqrt{\text{counts}}}{t(\text{mins})} .$$

$$Q = 20 \text{ gms of silver iodide/hr}$$

where there are 4×10^{15} particles/gm (effective -20°C), this gives,

$$Q = 2.2 \times 10^{13} \text{ particles/sec} .$$

A typical 24 hr seeding operation uses two generators so,

$$Q_m + Q_R = Q_T = 4.4 \times 10^{13} \text{ particles/sec}$$

assuming that the sources are again additive. Optimum $\overline{\chi}$ values may vary from 5 to 100 part./liter and with $\overline{U} \sim 10$ m/s,

$$\frac{\overline{\chi}\,\overline{U}}{Q} \sim 1 \times 10^{-9}\text{m}^{-2} \text{ to } 23 \times 10^{-9}\text{m}^{-2} .$$

During seeding operations observable nuclei on Chalk Mountain may vary from 5 to 300 part./liter or

$$\frac{\overline{\chi}\,\overline{U}}{Q} \sim 1 \times 10^{-9}\text{m}^{-2} \text{ to } 68 \times 10^{-9}\text{m}^{-2} .$$

The agreement between model and field is rather good however the model concentrations values are perhaps somewhat lower than is observed during a seeding operation, yet tentative analysis of dispersion data for the airflow with neutral stability suggests concentration values on the order of $30 \text{ to } 35 \times 10^{-9}\text{m}^{-2}$ near Chalk Mountain which improves the agreement between model and field twofold.

A very important aspect of the dispersion problem is whether sufficient artificial nuclei are being delivered to storm cloud systems in the Eagle River and Climax area. Cloud bases during storm conditions are near the 12,000 ft level and lower. This is approximately 1200 meters above our reference height of 2377 (7800 ft) meters. Figure 20 shows the approximate cloud volume above 12,000 ft occupied by tracer material from the Redcliff source for the barostromatic airflow case.

This indicates that some portion of the orographic cloud system receives artificial nuclei but with varying concentrations. Yet, much of the seeding material remains near the surface. In the prototype, thermal convection, changing stability, and variable wind directions could possibly bring additional material upward into the cloud systems.

b. Seeding generator locations

Model and field measurements confirm that seeding nuclei are reaching the target area from the Redcliff and Minturn sources. Reevaluation may be necessary regarding the location of the Redcliff generator especially during very stable or inversion conditions. If the target area includes the Chicago Ridge complex and surrounding area this may not be a problem.

The Minturn generator location appears to be satisfactory because of its location with respect to the downstream Battle Mountain ridge. Additional generator sites may be necessary if a larger target area is under consideration. Model experiments could help in the decision making related to the selection of such sites.

D. Numerical Simulation

The basic problem for obtaining numerical results for aerosol (e.g., silver iodide) dispersion is solving for the wind velocity distributions over the irregular terrain and then the concentration distributions of the aerosol.

Our first attempt was a two dimensional computer model based on the perturbation equation of Scorer (1955),

$$\frac{\partial^2 w}{\partial z^2} + \frac{\partial^2 w}{\partial x^2} + \left(\frac{g\beta}{U^2} - \frac{\partial^2 U/\partial z^2}{U}\right)w = 0 \quad . \tag{30}$$

Due to a unsatisfactory numerical scheme for solving equation (30) the solution for the air motion over irregular terrain was not reasonable.

Although other investigations have been able to generate wind velocity distributions by using Scorer's perturbation equation an analysis of the problem suggests a more realistic approach such as using the basic equations of mechanics and thermodynamics.

A second approach to the problem was attempted using the following equations,

Two-dimensional equations of motion

$$\begin{aligned} \frac{du}{dt} &= -\frac{1}{\rho}\frac{\partial p}{\partial x} + K_M \nabla^2 u \\ \frac{dw}{dt} &= -\frac{1}{\rho}\frac{\partial p}{\partial z} - g + K_M \nabla^2 w \quad . \end{aligned} \tag{31}$$

Thermodynamic equation

$$\frac{d\theta}{dt} = K_H \nabla^2 \theta \quad . \tag{32}$$

Equation of continuity

$$\frac{\partial u}{\partial x} + \frac{\partial w}{\partial z} = 0 \quad . \tag{33}$$

Turbulent diffusion equation

$$\frac{\partial \chi}{\partial t} + \frac{\partial(\psi,\chi)}{\partial(x,z)} = \frac{\partial}{\partial x}(K_x \frac{\partial \chi}{\partial x}) + \frac{\partial}{\partial z}(K_z \frac{\partial \chi}{\partial z}) + Q \quad . \tag{34}$$

For computational purposes Ogura (1963) and Orville (1967) have modified the equation of motions into a vorticity equation,

$$\frac{\partial \eta}{\partial t} + \frac{\partial(\psi,\eta)}{\partial(x,z)} = g \frac{\partial \phi}{\partial x} + K_M \nabla^2 \eta \tag{35}$$

where the second term is advection, the third, temperature buoyancy and fourth is the turbulent mixing term. A stream function is defined by,

$$u = - \frac{\partial \psi}{\partial z} , \quad w = \frac{\partial \psi}{\partial x} \tag{36}$$

and the vorticity is defined by

$$\eta = \frac{\partial w}{\partial x} - \frac{\partial u}{\partial z} \tag{37}$$

therefore

$$\nabla^2 \psi = \eta \quad . \tag{38}$$

The thermodynamic equation is modified to,

$$\frac{\partial \phi}{\partial t} + \frac{\partial(\psi,\phi)}{\partial(x,z)} = K_H \nabla^2 \phi \tag{39}$$

where $\phi = \frac{\theta'}{\bar{\theta}}$.

Fosberg (unpublished manuscript) has modified the vorticity and thermodynamic equations further by expressing them in linearized form. These equations are:

Thermodynamic equation

$$\frac{\partial \phi}{\partial t} + \bar{u} \frac{\partial \phi}{\partial x} + u' \frac{\partial \phi}{\partial x} + \bar{w} \frac{\partial \phi}{\partial z} + w' \frac{\partial \phi}{\partial z} - K_H \nabla^2 \phi = 0 \quad . \tag{40}$$

Vorticity equation

$$\frac{\partial \eta'}{\partial t} + \bar{u} \frac{\partial \eta'}{\partial x} + u' \frac{\partial \eta'}{\partial x} + \bar{w} \frac{\partial \eta'}{\partial z} + w' \frac{\partial \eta'}{\partial z} - K_M \nabla^2 \eta' - g \frac{\partial \phi}{\partial x} + g \frac{\partial \phi}{\partial z} = 0 \quad . \tag{41}$$

Thus, the linearized vorticity and thermodynamic equations with boundary conditions form the basis of the numerical model for generating the velocity distributions over irregular terrain. The turbulent diffusion equation has not been incorporated into this present model because restricted funding has curtailed progress in the programming aspects of this problem.

So far we have only considered two-dimensional computer models for the dispersion problem. A three-dimensional computer model would provide a more realistic approach to dispersion over irregular terrain. A solution of a three-dimensional computer model is now feasible with the larger computers. An example of such a model is given by Hino (1968).

E. Conclusions

This has been the first time that a dry ice barostromatic airflow has been documented by temperature and velocity profile measurements. Similarity analysis shows that Reynolds, Prandtl, Euler, Eckert and Richardson numbers need to be the same for model and prototype for this type of flow. Comparison of limited field data of temperature and wind fields with data obtained over the Eagle River Valley-Chalk Mountain topographic model show that Reynolds, Prandtl and Richardson number similarity can be satisfied. Richardson number criteria appears to be the most important for the dispersion problem. Euler and Eckert number similarity cannot be achieved at this time but are of lesser importance to the dispersion problem.

A problem regarding the effect of the carbon dioxide on the density stratification has not been considered here but future experiments will attempt to measure this variable. Another problem which may effect the temperature or density stratification is the heat flux interchange between topographic model and flowing air. According to the equation of heat transfer from earth,

$$Q_T - Q_R + Q_{L\downarrow} - Q_{L\uparrow} = \pm Q_G \pm Q_H \pm Q_E \qquad (42)$$

where under under normal fair weather days each term may make a contribution. However, the weather situation of interest during artifical seeding operations in the Climax area is storm periods with fairly extensive cloud cover over the region. In this case, Q_T , Q_R , $Q_{L\downarrow}$, $Q_{L\uparrow}$ and Q_G may be assumed negligible. Q_H and Q_E maybe of importance since the airflow could be warmer or colder than the underlying surface.

For the topographic model during this experimental period the airflow was colder than the model and a possible heat flux into the airflow may have been present. The temperature distribution over the model (Fig. 13) shows a near neutral stability layer in the lower levels over most of the model, most likely due to the heat flux from the warmer model. The effect of this temperature feature on the dispersion data is difficult to evaluate but it could contribute to lifting of the tracer material from the surface of the model. Altogether this aspect is not detrimental to the modeling technique, in fact, if it is possible to control the temperature of the airflow and model surface a wider range of environmental conditions could be simulated.

Several other similarity problems could be listed but these are not essential to this report at this time. Future work will report on these problems.

Radioactive gas concentration measurements taken during barostromatic airflow conditions indicate that average concentration values, plume widths, and heights may be possible parameters that can be estimated from model experiments. Limited field measurements of ice nuclei concentrations at Chalk Mountain show a variation of 5 to 300 part./liter or

$$\frac{\overline{\chi}\,\overline{U}}{Q} \sim 1 \times 10^{-9} m^{-2} \quad \text{to} \quad 68 \times 10^{-9} m^{-2} .$$

Concentration values deduced from radioactive gas measurements over the topographic model show values within the same range,

$$\frac{\overline{\chi}\,\overline{U}}{Q} \sim 15 \times 10^{-9} m^{-2} \quad \text{to} \quad 18 \times 10^{-9} m^{-2} .$$

Future experiments should improve on these results.

It should be emphasized that these measurements were obtained under two important assumptions: 1) No directional wind shear except what is generated by terrain features and 2) Incompressible flow. Field dispersion measurements should help us determine what possible effects these two assumptions have on the model results.

F. Future Work

1. Model construction

The next topographic model to be constructed will simulate the southwest wind direction in the San Juan Mountain area. The Wolf Creek Pass region has been selected as the area to be modeled. This mountain barrier will be a blocking type. Scale and construction methods have not been established at this time.

2. Laboratory experiments

a. Elk Mountain model (southwest flow)

A topographic model of Elk Mountain is now available for wind tunnel work. This mountain is relatively isolated from other large mountains and its geometry is relatively simple. Wind tunnel experiments using the Colorado State University low speed wind tunnel will commence this Fall. Transport and dispersion patterns will be those for a singular mountain in contrast to the complex topography found in the Eagle River-Climax area.

b. Eagle River-Chalk Mountain model (northwest flow)

A short experimental period in the Colorado State University low speed wind tunnel will attempt to measure carbon dioxide concentrations and improve measurement of velocity profiles using the smoke wire system.

c. Wolf Creek Pass model (southwest flow)

Due to the large area coverage of this topograhic region, wind tunnel experiments will be conducted in the new large wind tunnel (7 ft x 12 ft). Both neutral stability and barostromatic airflow will be attempted as well as dispersion measurements.

3. Field work

a. Eagle River-Chalk Mountain area

Observations and analysis of surface and upper-level data will continue during this period for making direct field comparisons with the wind tunnel results. The observations to be included will be,

1) Rawin-or radiosonde, pilot balloon, and superpressure balloon data. These data will help determine the vertical structure of the atmosphere in orographic terrain.
2) Surface temperature, humidity, pressure, and above surface turbulence data obtained at field weather stations for different elevations approaching Chalk Mountain will assist in defining the characteristics of the orographic airstream.

Field dispersion data from silver iodide instruments and other methods will be used to help verify the model dispersion results.

b. Elk Mountain area

The University of Wyoming water resources group would be required to furnish the necessary prototype data. This will require obtaining rawin or radiosonde, pilot balloon, superpressure balloon, and dispersion data. Some of this data is avaliable now.

c. Wolf Creek area

Initial rawin or radiosonde and pilot balloon data should be obtained to assist in defining similarity criteria for the model experiments.

G. Appendix

The following personnel were associated with the research project during the period under review:

1. Professional staff

Name	Project responsibility
J. E. Cermak	Principal investigator
L. O. Grant	Coordinated field program with laboratory experiments
M. M. Orgill	Supervised laboratory experiments, and analysis of data; assisted in obtaining field data; numerical simulation
J. A. Garrison	Assisted with laboratory experiments
L. Hjermstad	Directed field data collection program
G. Wooldridge	Assisted in obtaining field data
C. Chappell	Assisted in obtaining field data
W. Kamm	Computer programming
Mrs. M. Working	Computer programming

2. Graduate research assistants and student help

R. Derickson	Laboratory experiments and data reduction
D. Nambudripad	Data reduction
S. Brown	Field work
R. Potter, III	Construction of models
W. Tully	Construction of models and data reduction
Mrs. S. Kulkarni	Data reduction

Name	Project responsibiltiy
3. Technical assistance	
B. Johnson	Construction of smoke wire circuit
J. Buckley	Construction of smoke wire
4. Western Scientific Service, Inc. (sub-contractor)	
J. Jones	Field work and data reduction
P. Hayes	Field work
D. Cobb	Field work
J. Price	Field work
5. Other assistance (not funded by project)	
G. Hsi	Assisted with laboratory experiments
D. Kesic	Assisted with laboratory experiments
F. Chaudhry	Assisted with laboratory experiments
S. P. S. Arya	Assisted with laboratory experiments

References

Abe, M., 1941: Mountain clouds, their forms and connected air current, Part II. Bull. Central Met. Observatory of Japan, VII, 3, pp.93-145.

Batchelor, G. K., 1953: The conditions for dynamical similarity of motions of a frictionless perfect- gas atmosphere. Quart. J. R. Met. Soc., Vol. 79, pp. 224-235.

Cermak, J. E., and J. Peterka, 1966: Simulation of wind field over Point Arguello, California, by wind-tunnel flow over a topographic model. Report No. CER65JEC-LAP-64, Fluid Dynamics and Diffusion Laboratory. Colorado State University.

Cermak, J. E., et al., 1968: Research and development technique for estimating air flow and diffusion parameters in connection with the atmospheric water resouces program. Progress Report No. 1, Contract No. 14-06-D-6455, Fluid Mechanics Program, Dept. of Civil Engineering, Colorado State University.

Cermak, J. E., L. O. Grant, and M. M. Orgill, 1969: Research and development technique for estimating airflow and diffusion parameters in connection with the atmospheric water resources program. Interim Report, CER68-69JEC-LOG-MMO-27, Fluid Dynamics and Diffusion Lab., Colorado State University.

Chappell, C. F., 1967: Cloud seeding opportunity recognition. Atmospheric Science Technical Paper 118, Dept. of Atmos. Sci., Colorado State University.

Chaudhry, F. H., 1969: Diffusion in a thermally stratified shear layer. Unpublished doctoral dissertation, Department of Civil Engineering, Colorado State University.

College of Engineering, 1966: Fluid Mechanics Program. Fluid Dynamics and Diffusion Laboratory, Colorado State University, p. 36.

Faires, R. A., and B. H. Parks, 1960: Radioisotope Laboratory Techniques, George Newnes Ltd., London, p. 129.

Grant, L. O., and P. W. Mielke, Jr. 1967: A randomized cloud seeding experiment at Climax, Colorado, 1960-65. Proceedings of the Fifth Berkeley Symposium on Mathematical Statistics and Probability, 5, pp. 115-131.

Grant, L. O., C. F. Chappell, and P. W. Mielke, Jr. 1968: The recognition of cloud seeing opportunity. Proceedings of the First National Conference on Weather Modification, Albany, New York.

Grant, L. O., J. E. Cermak., and M. M. Orgill, 1968: Delivery of nucleating materials to cloud systems from individual ground generators. Proceedings of the Third Skywater Conference on the Production and Delivery of cloud nucleating materials, pp. 99-134.

Hino, M., 1968: Computer experiment on smoke diffusion over a complicated topography. Atmospheric Environment, Vol. 2, 6, pp. 541-558.

Ludlam, F. H., 1955: Artificial snowfall from mountain clouds, Tellus, 7, pp. 277-290.

Ogura, Y., 1963: The evolution of a moist convective element in a shallow, conditionally unstable atmosphere- A numerical calculation. J. Atmos. Sci., 20, pp. 407-424.

Orgill, M. M.: Wind tunnel models for estimating transport and dispersion in mountainous terrain. Unpublished doctoral dissertation, Dept. of Civil Engineering, Colorado State University.

Orville, G. D., 1967: The numerical modeling of mountain upslope winds and cumulus clouds. Report 67-2, Institute of Atmos. Sci., South Dakota School of Mines and Technology.

Reiter, E. R., and P. F. Lester, 1967: Dependence of the Richardson number on scale length. Atmos. Sci. Paper No. 111, Dept. of Atmos. Sci., Colorado State University.

Scorer, R. S., 1953: Theory of airflow over mountains, II: The flow over a ridge. Quart. J. R. Met. Soc., 79, pp. 70-83.

Scorer, R. S., 1955: Theory of non-horizontal adiabatic flow in the atmosphere. Quart. J. R. Met. Soc., 75, p. 41.

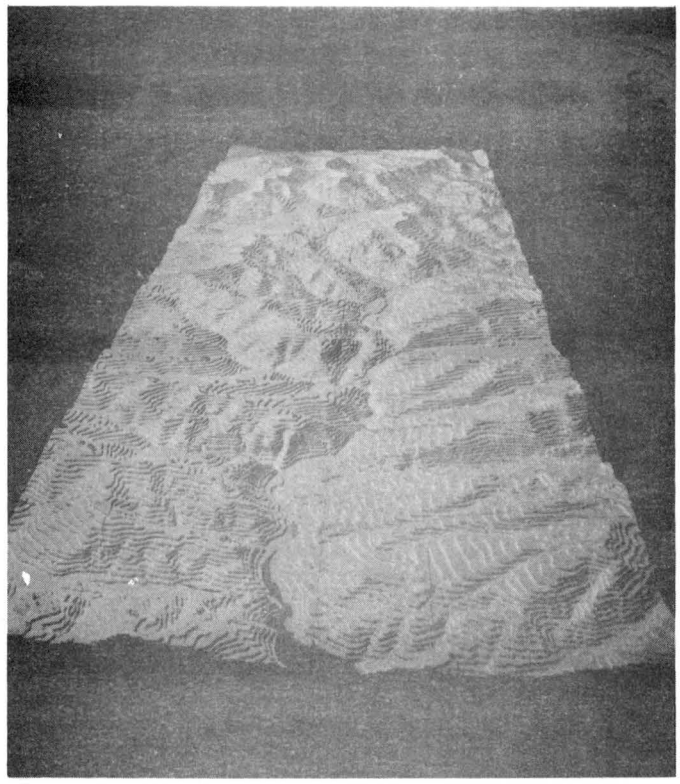

Looking downstream

Looking upstream

Figure 1 Eagle River Valley topographic model.

Figure 2 Topography of experimental area with generator locations.

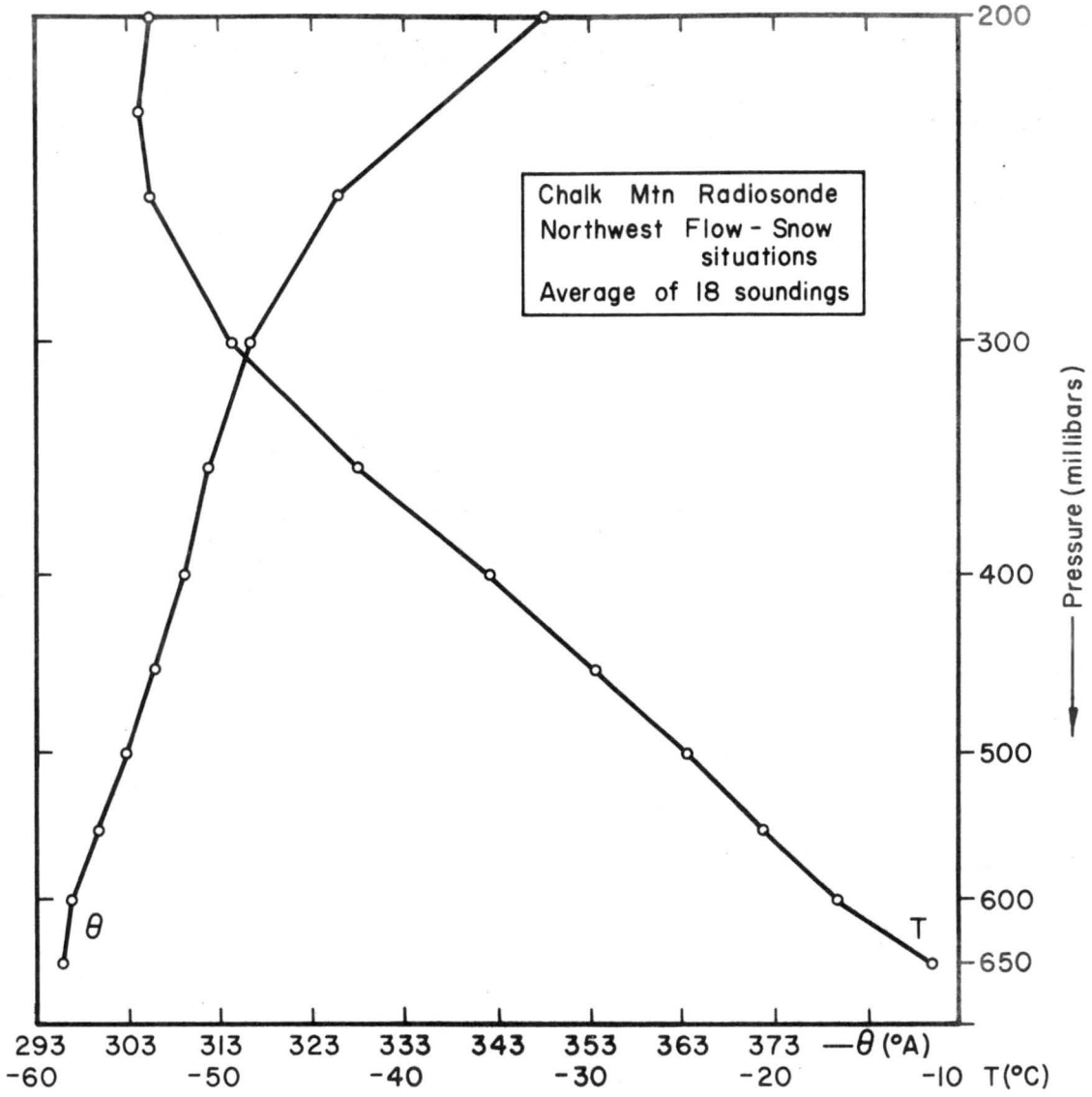

Figure 3 Mean temperature sounding for northwest flow (snow situations) at Chalk Mountain.

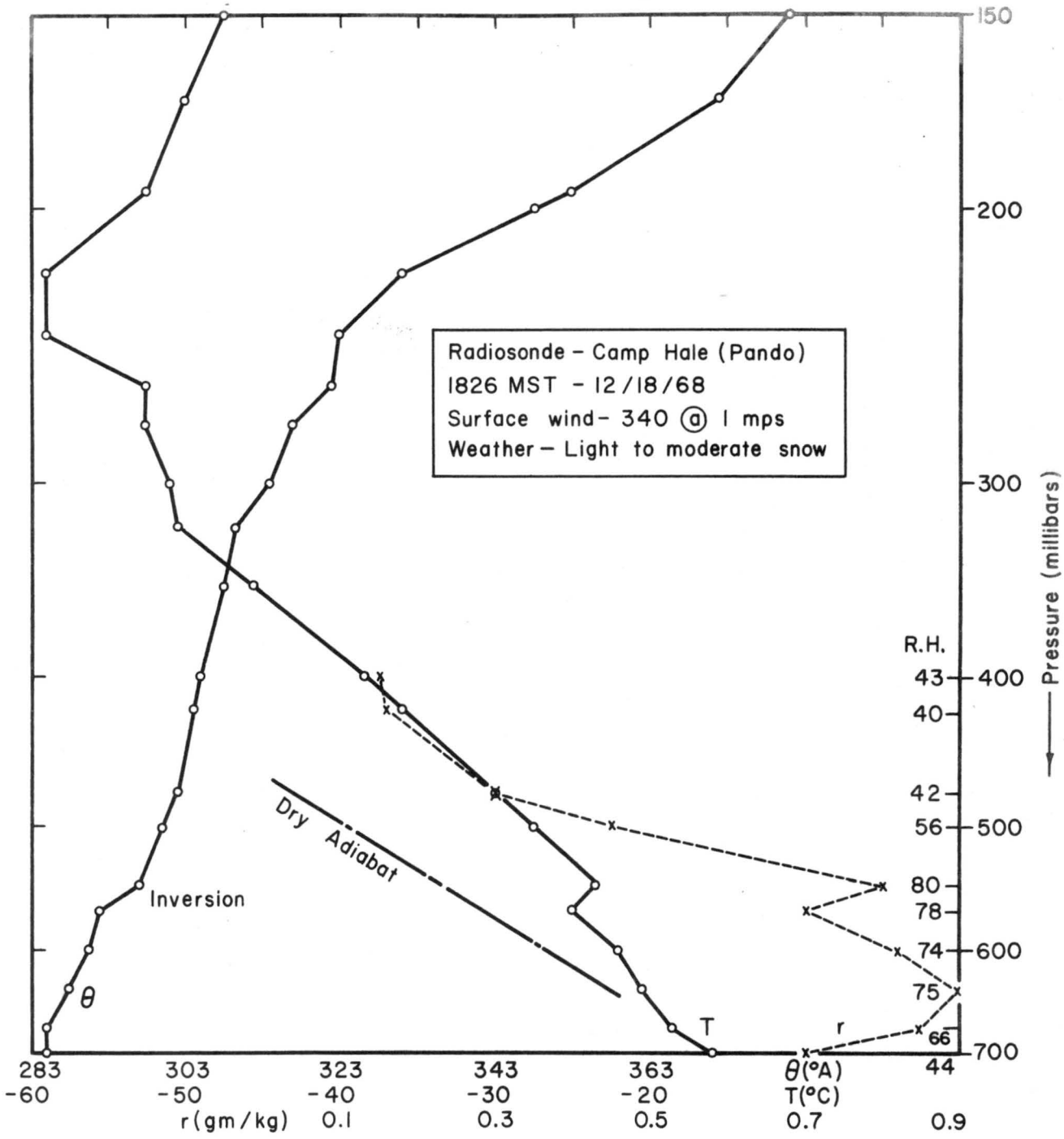

Figure 4 Temperature and humidity sounding during northwest flow at Camp Hale.

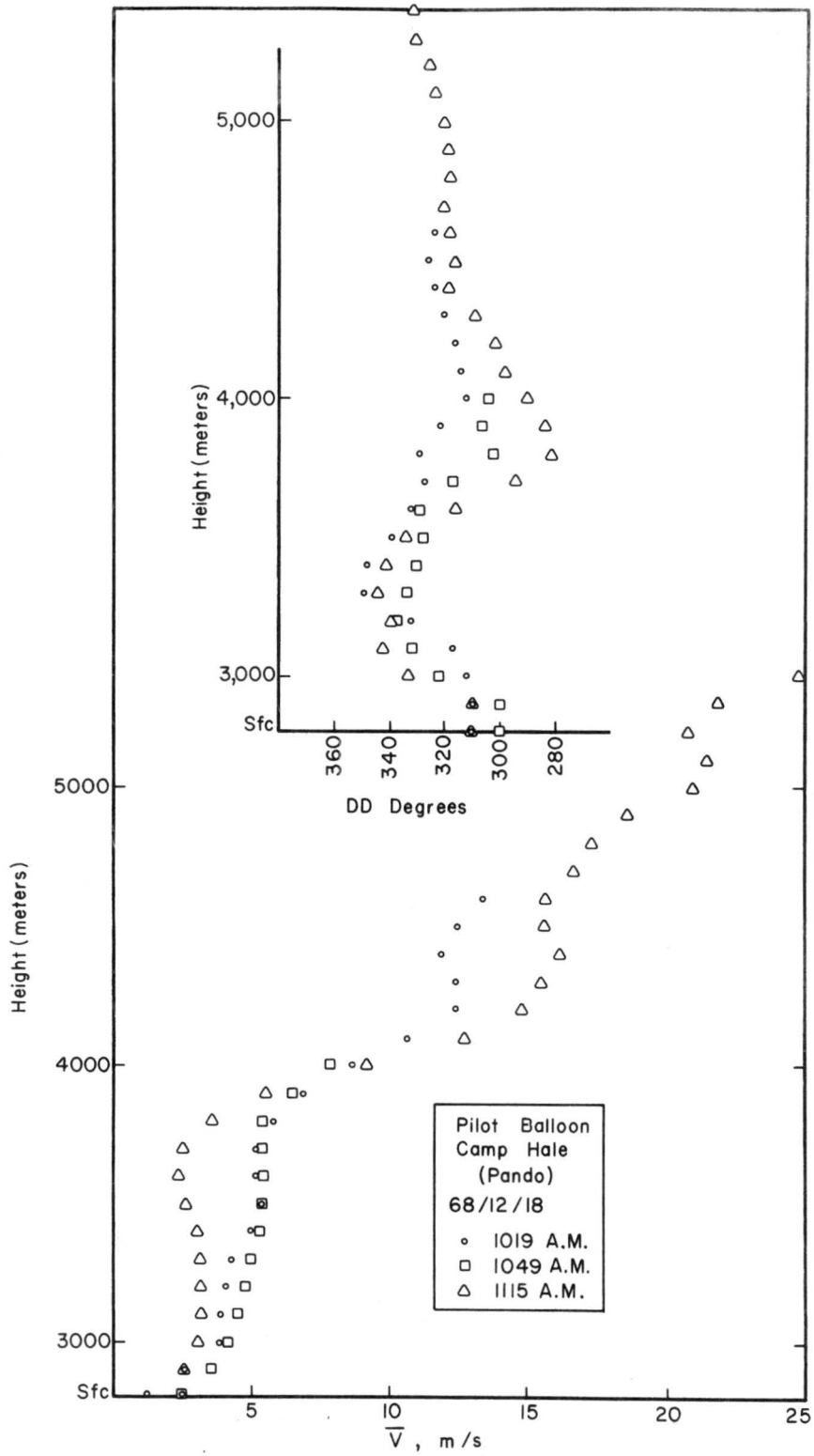

Figure 5 Pilot balloon observations at Camp Hale.

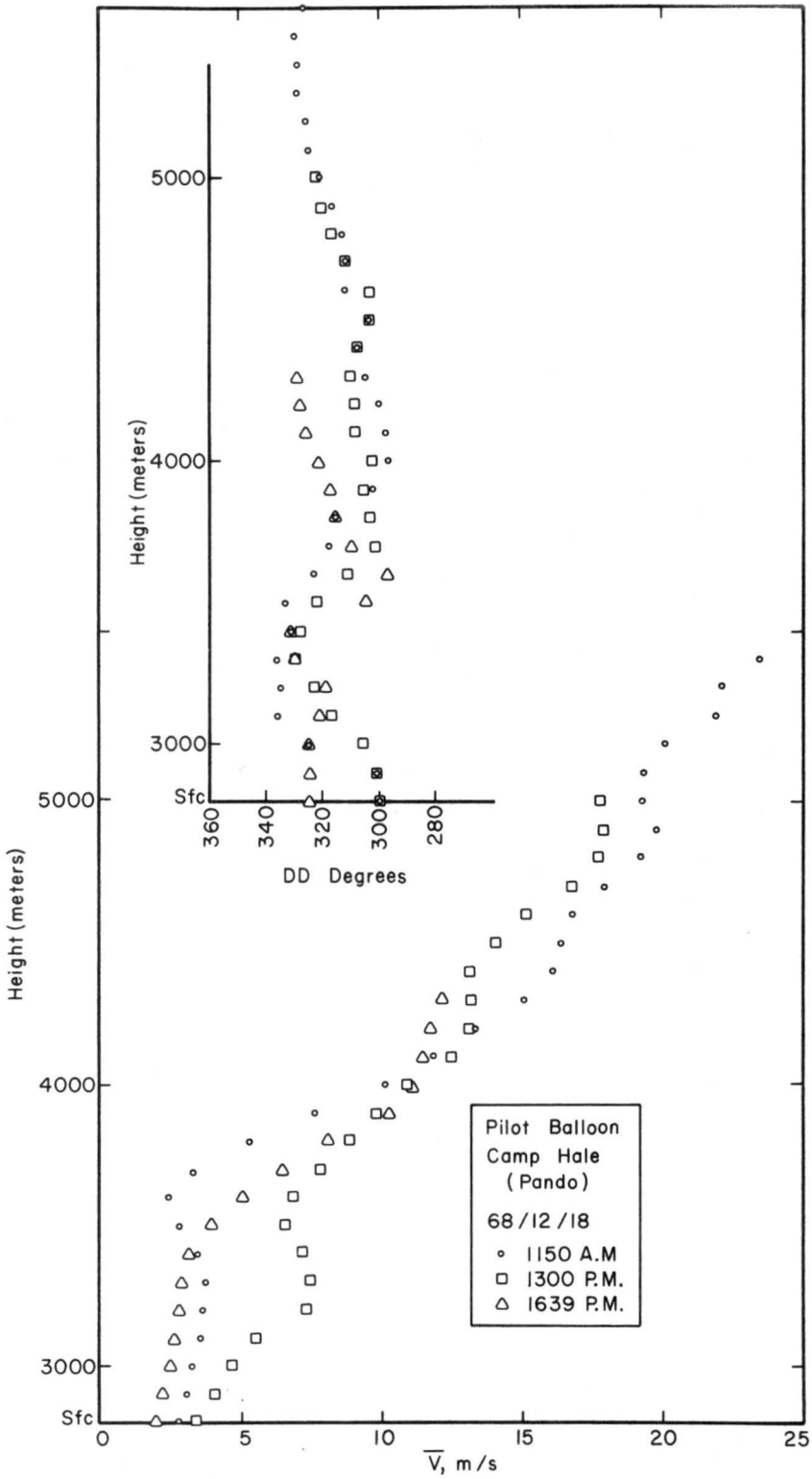

Figure 6 Pilot balloon observations at Camp Hale.

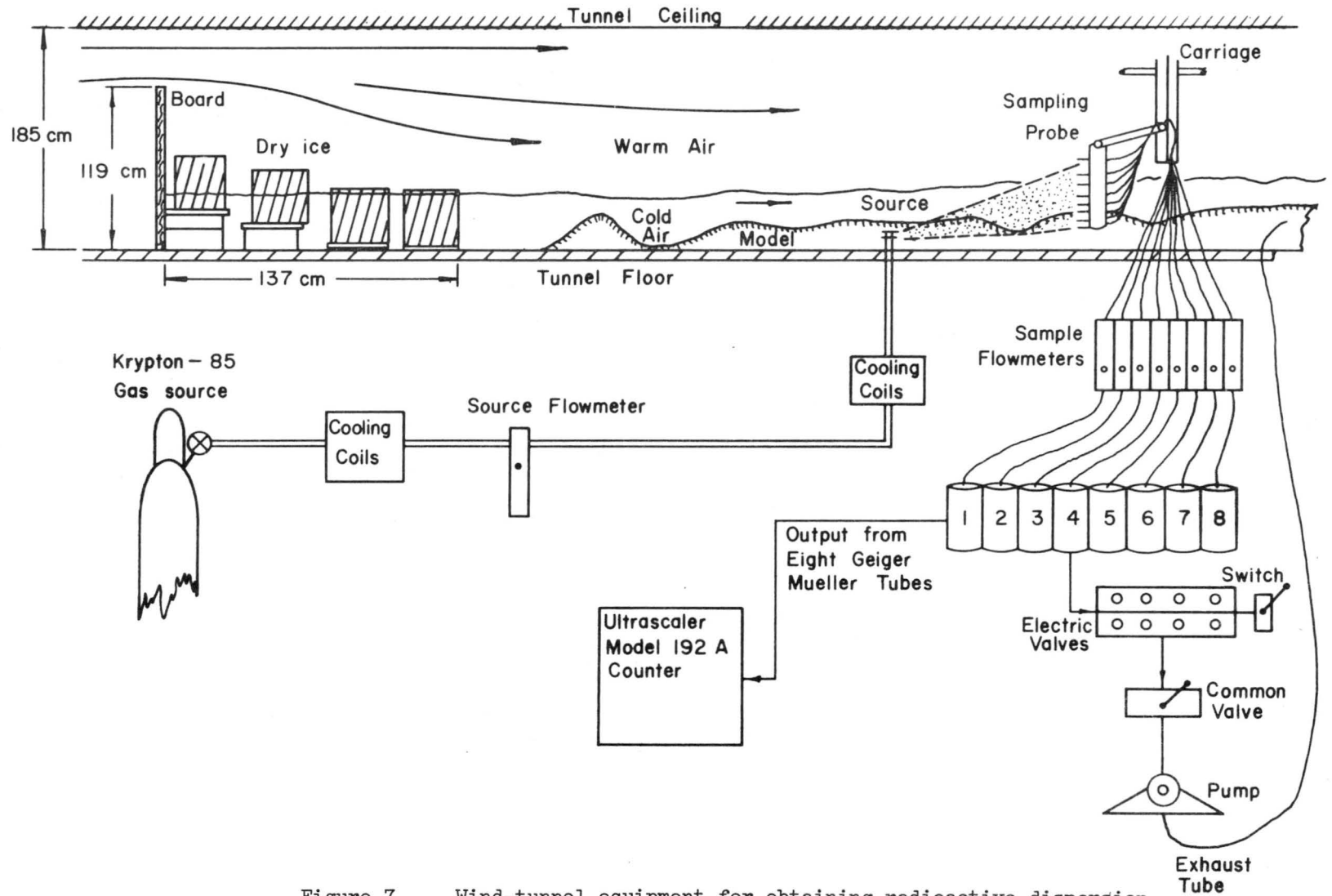

Figure 7 Wind-tunnel equipment for obtaining radioactive dispersion measurements for the barostromatic airflow case.

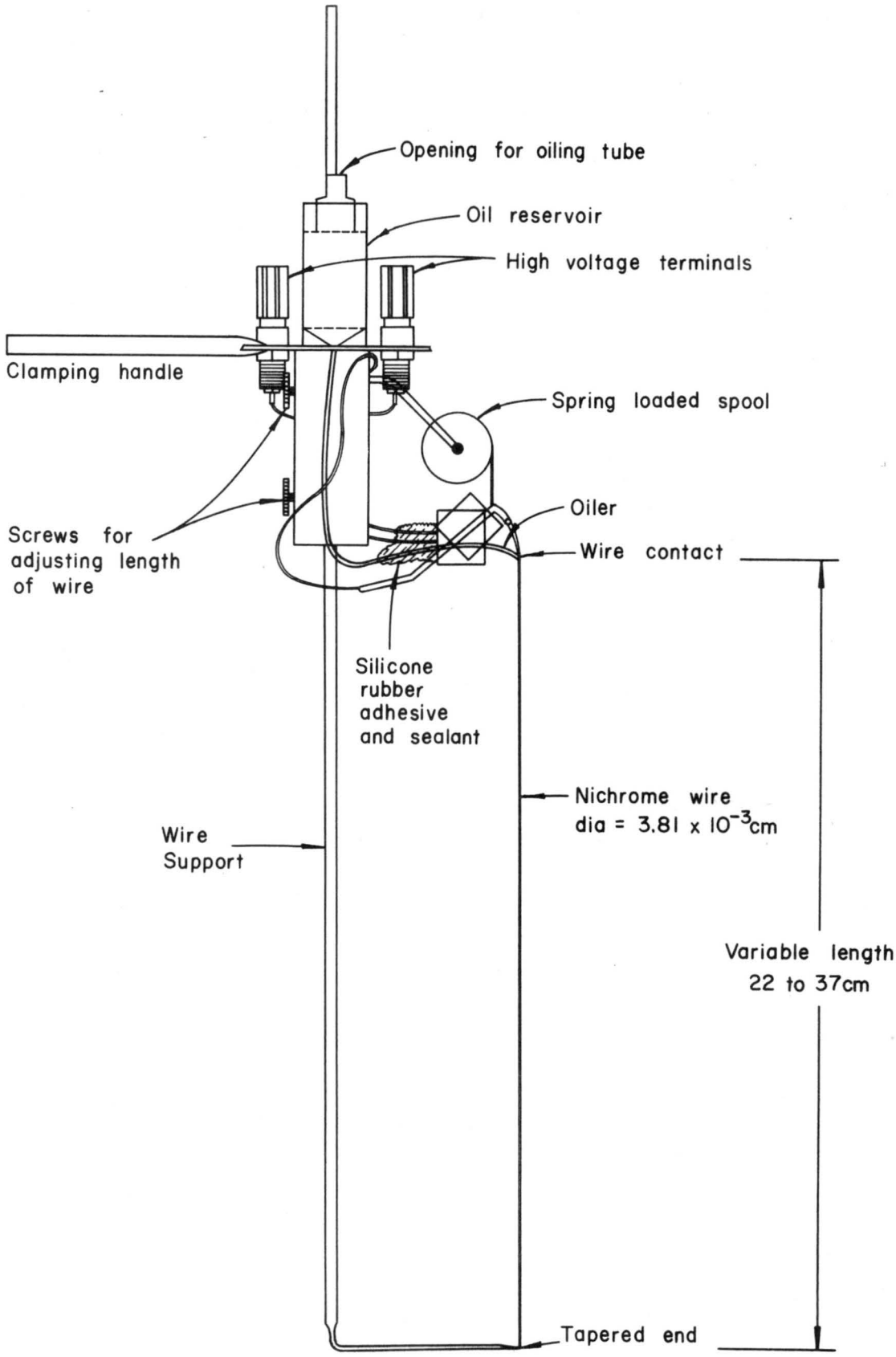

Figure 8 Smoke-wire probe for measuring low airflow case.

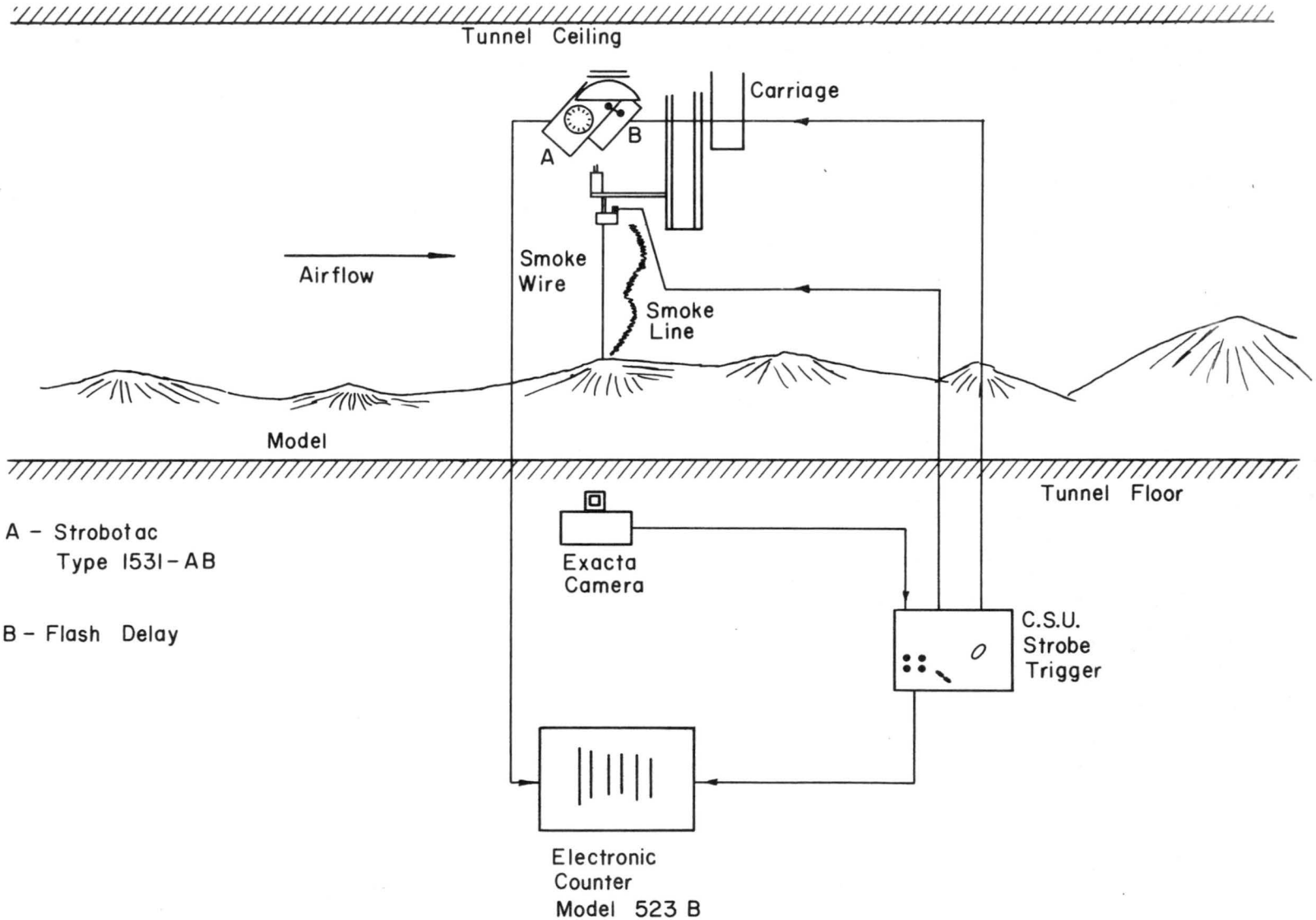

Figure 9 Smoke-wire system for obtaining low airflow velocities in a wind tunnel.

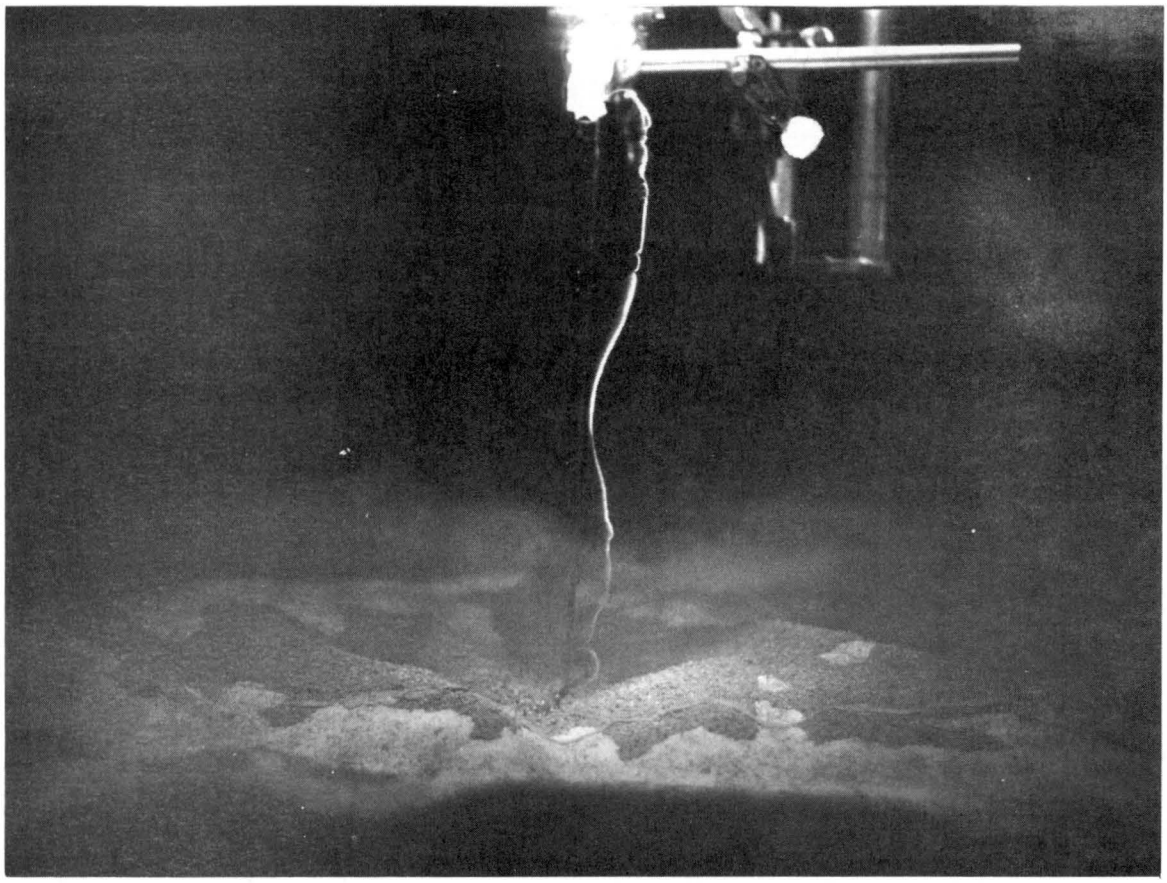

Figure 10 Smoke line obtained from the smoke wire probe.

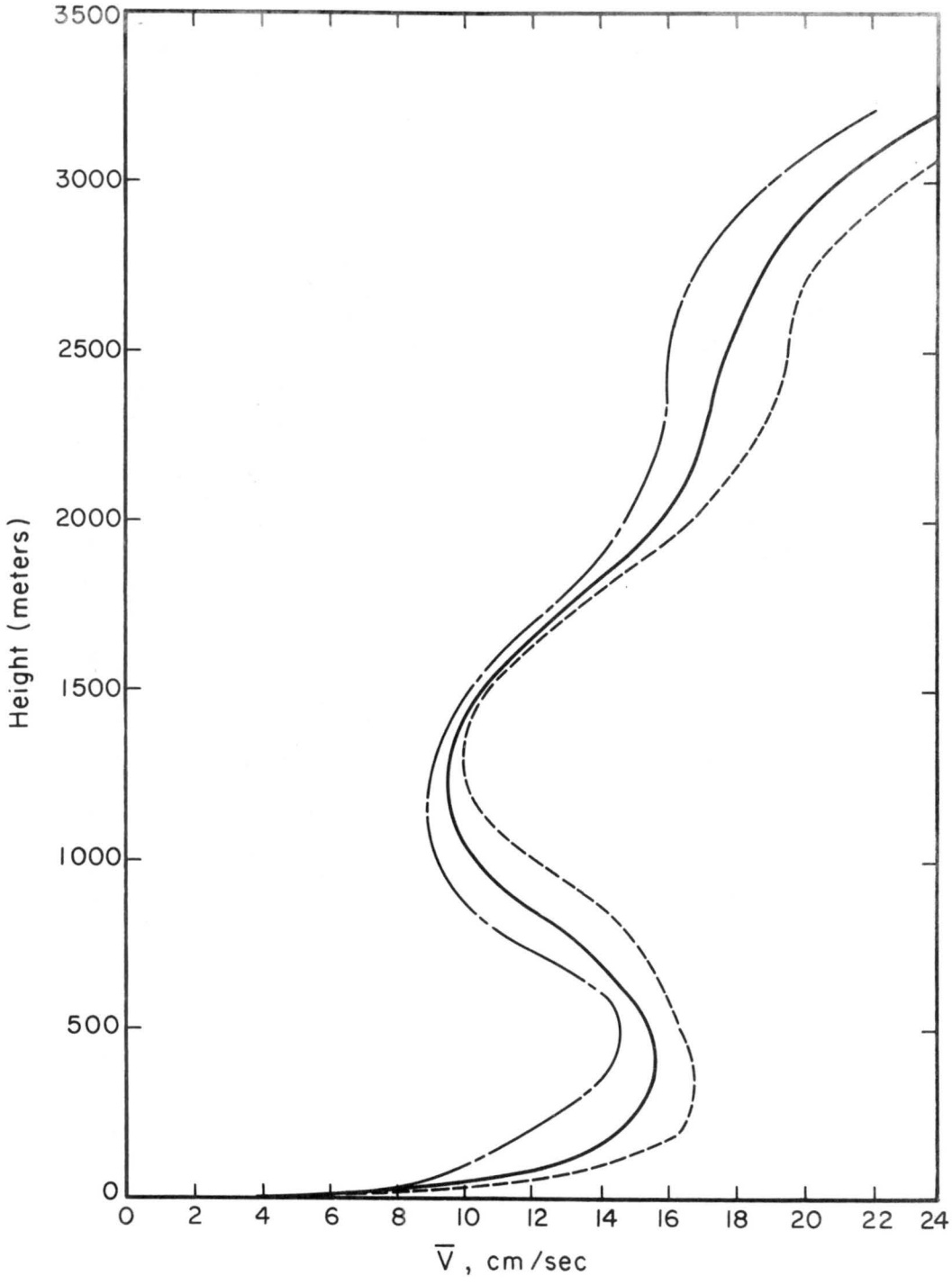

Figure 11 Three different picture frames of smoke-line velocity profiles obtained at the Camp Hale model site.

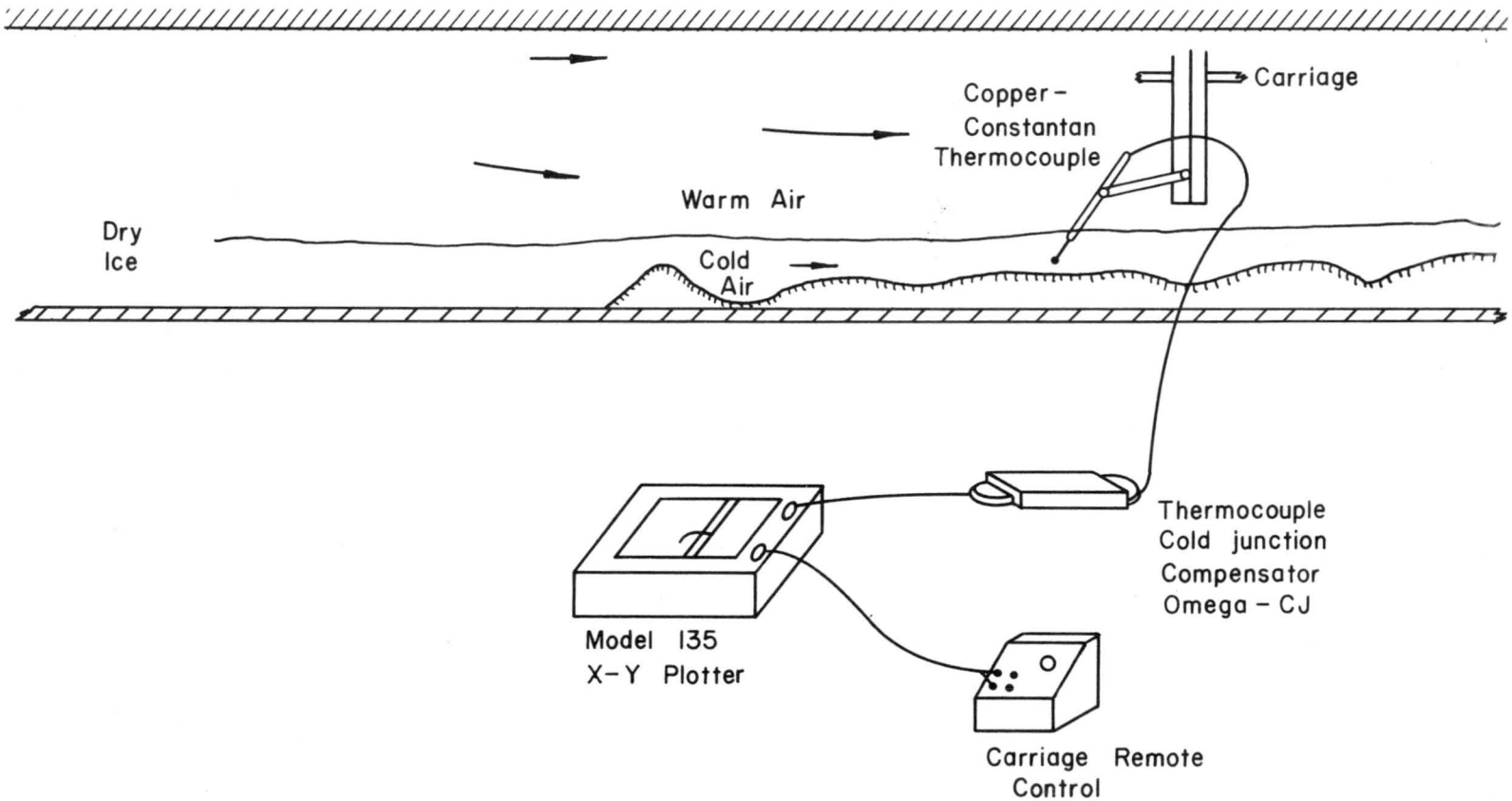

Figure 12 Temperature measuring instrumentation.

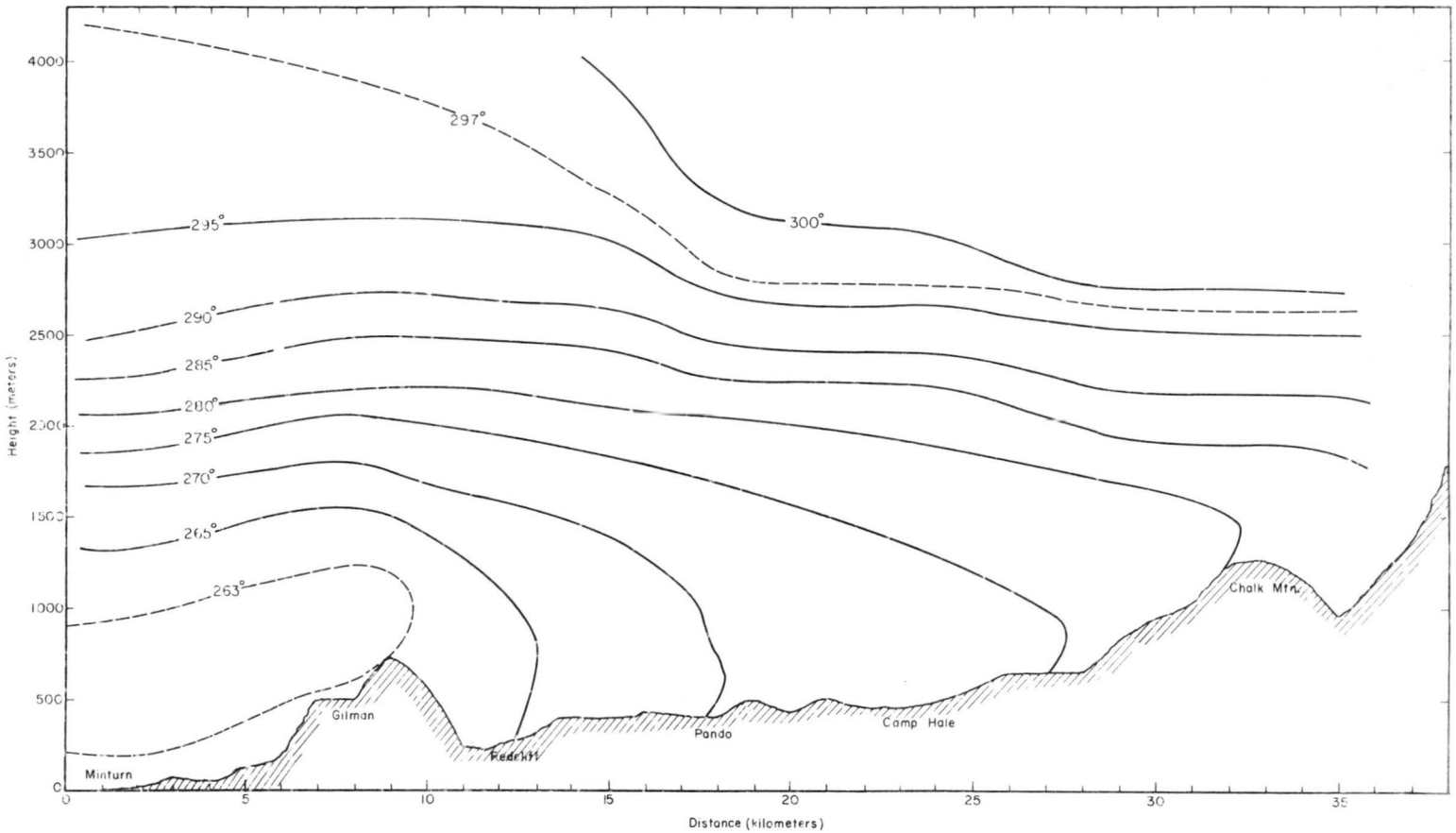

Figure 13 Temperature field (°Kelvin) over topographic model produced by dry ice.

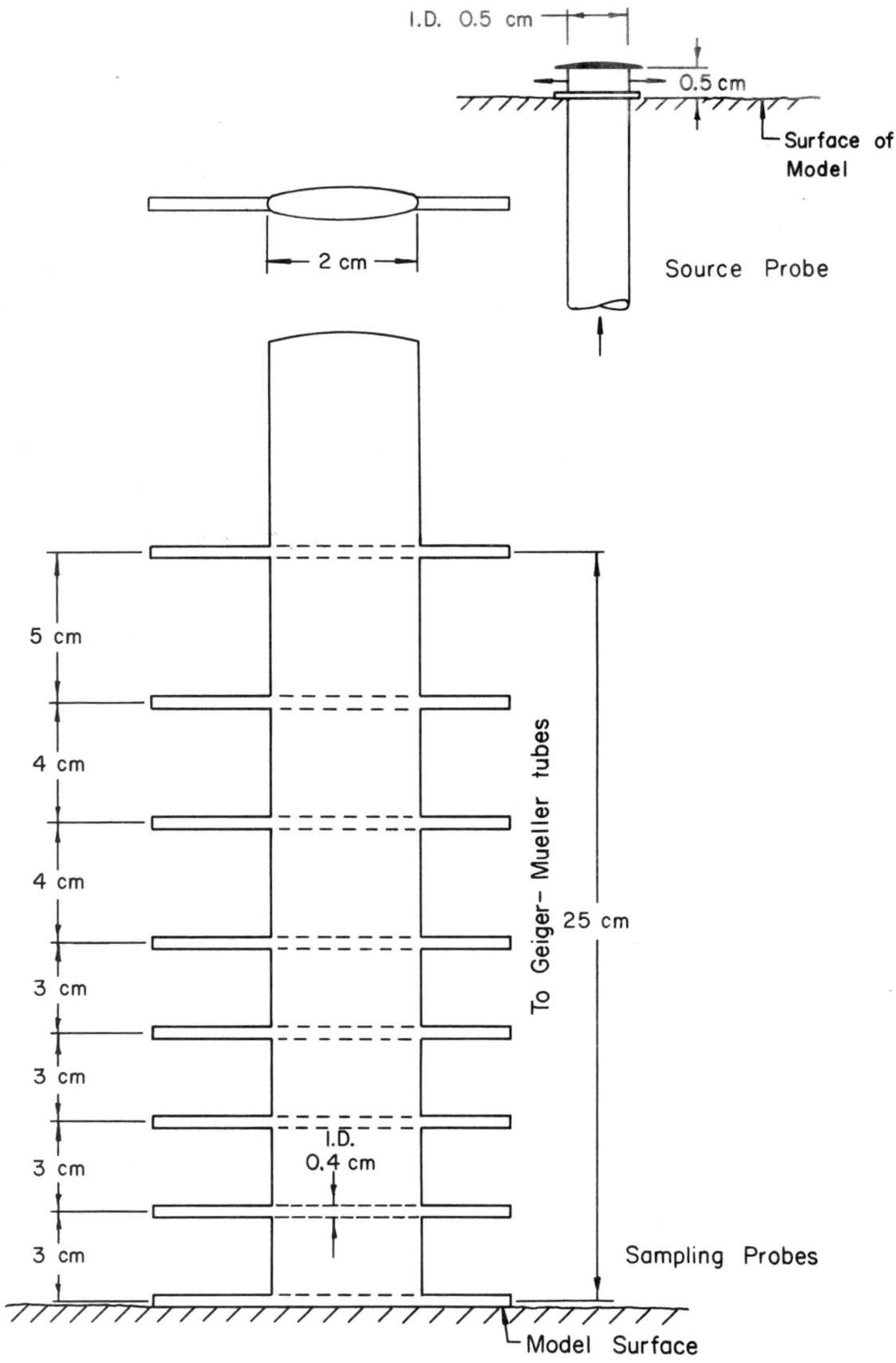

Figure 14 Source and sampling probes for radioactive dispersion experiments.

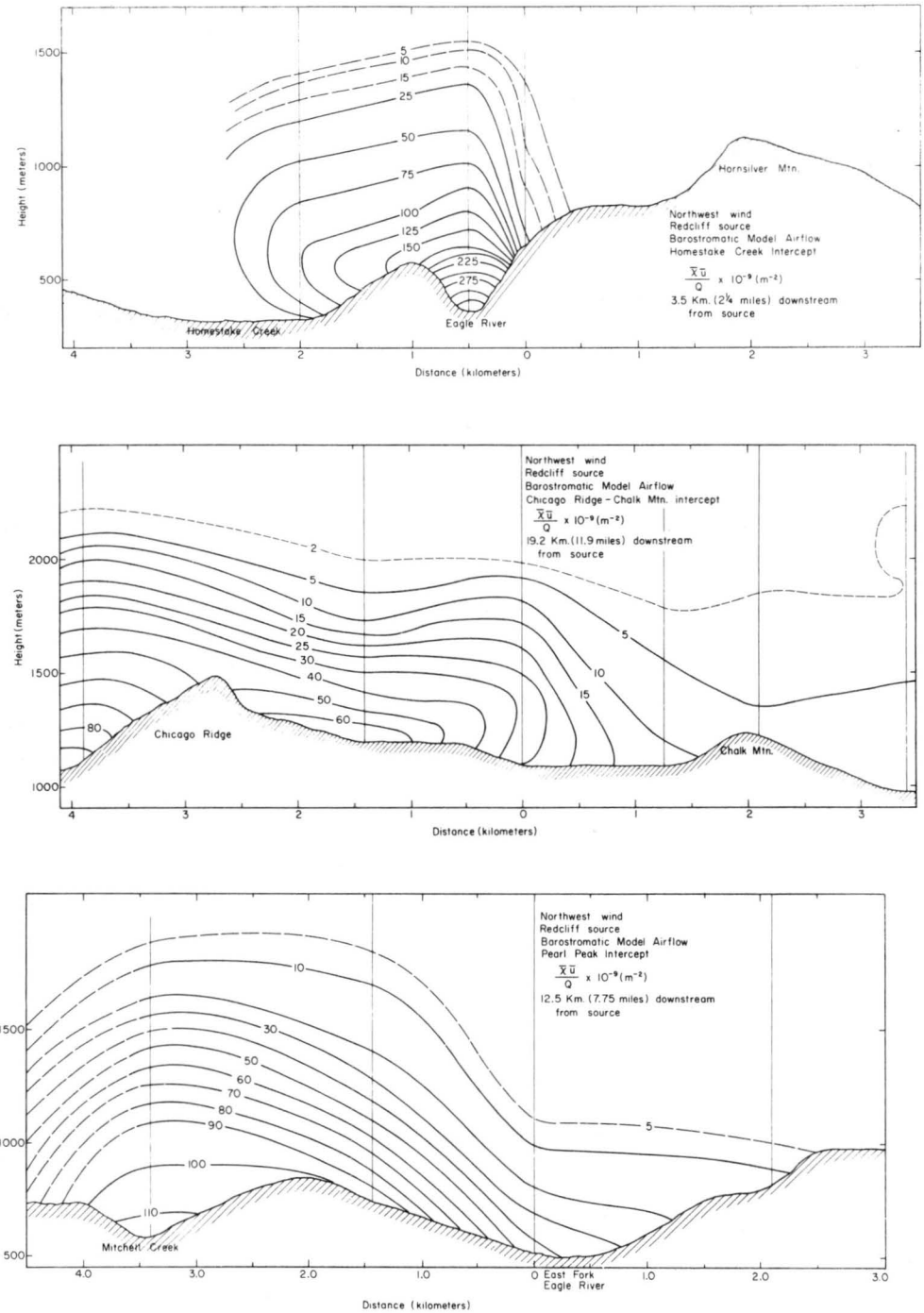

Figure 15 Lateral cross section of concentration parameter $\frac{\bar{\chi}\bar{U}}{Q}$ downwind from Redcliff source. Thin lines are measurement locations.

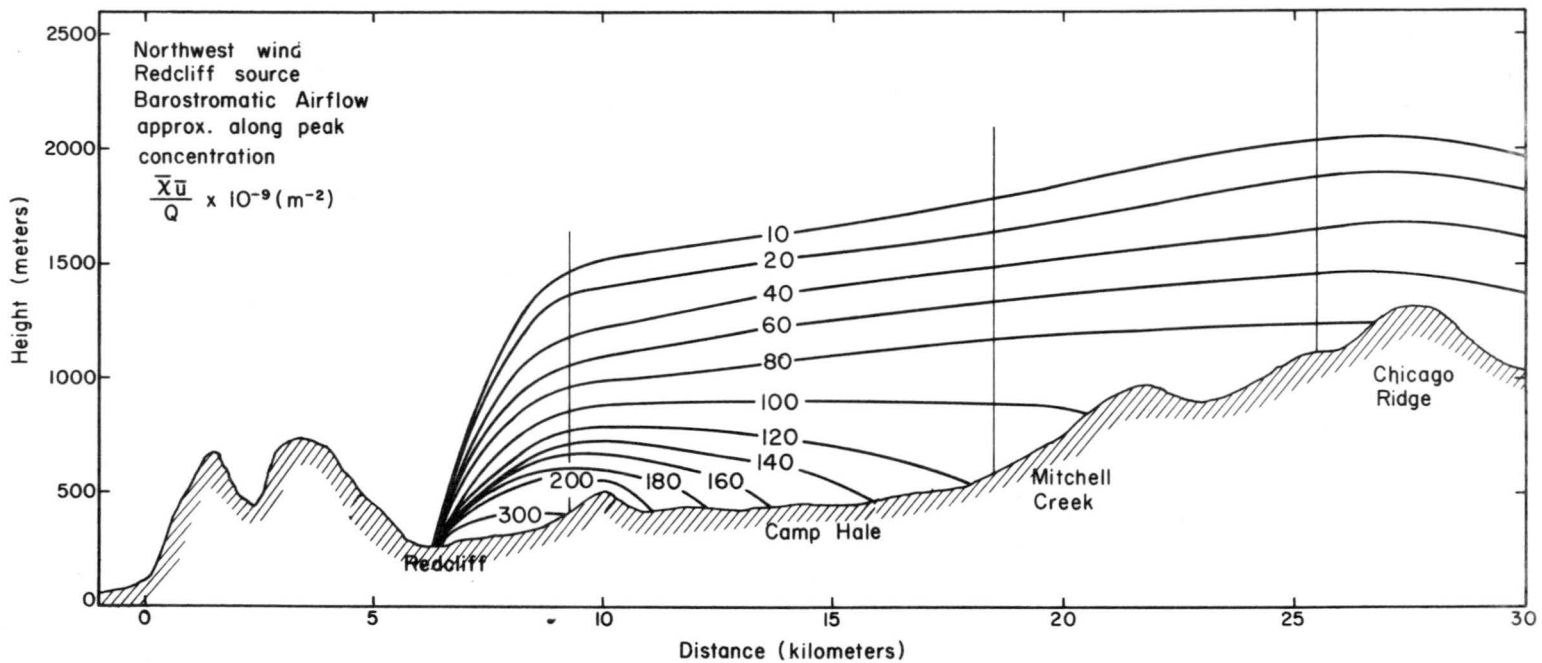

Figure 16 Vertical cross section of concentration parameter $\frac{\bar{\chi}\,\bar{U}}{Q}$ downwind from Redcliff source.

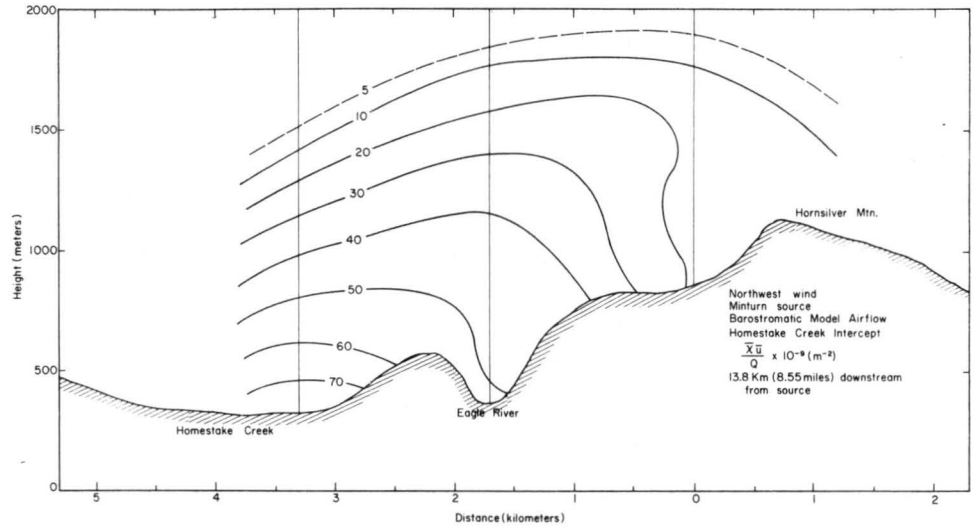

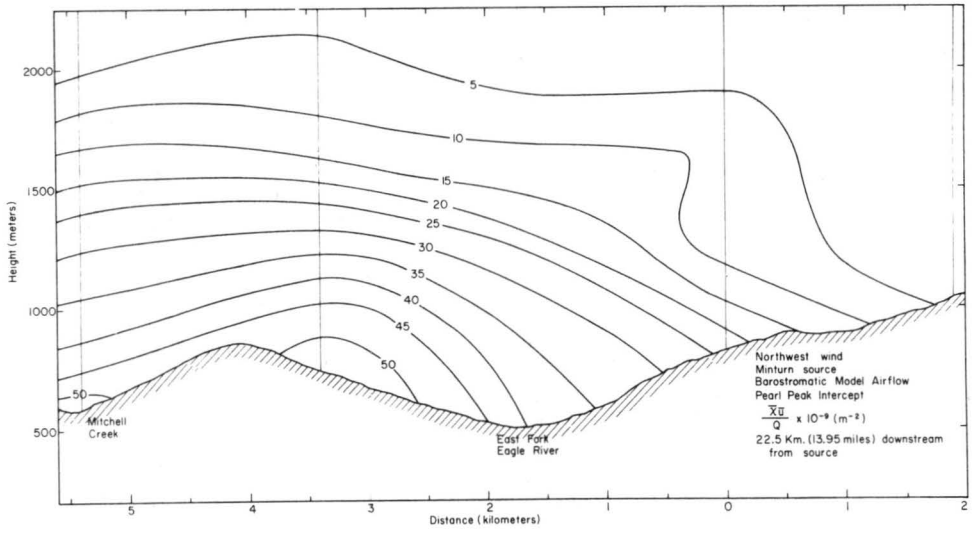

Figure 17 Selected lateral cross sections of concentration parameter $\frac{\overline{\chi}\,\overline{U}}{Q}$ downwind from Minturn source.

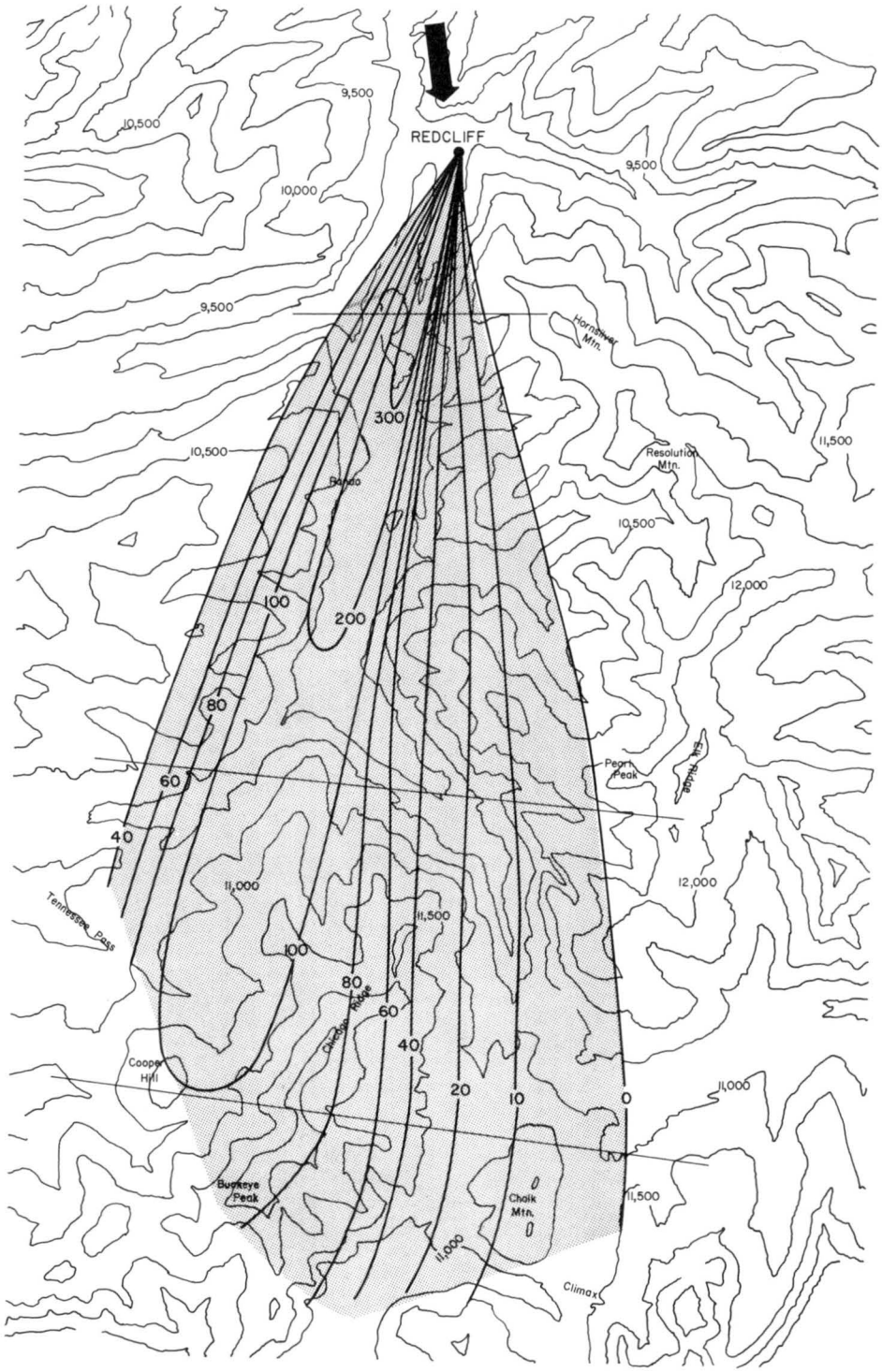

Figure 18 Surface concentration $\frac{\bar{\chi}\,\bar{U}}{Q} \times 10^{-9}(m^{-2})$ downwind from Redcliff source-Barostromatic airflow.

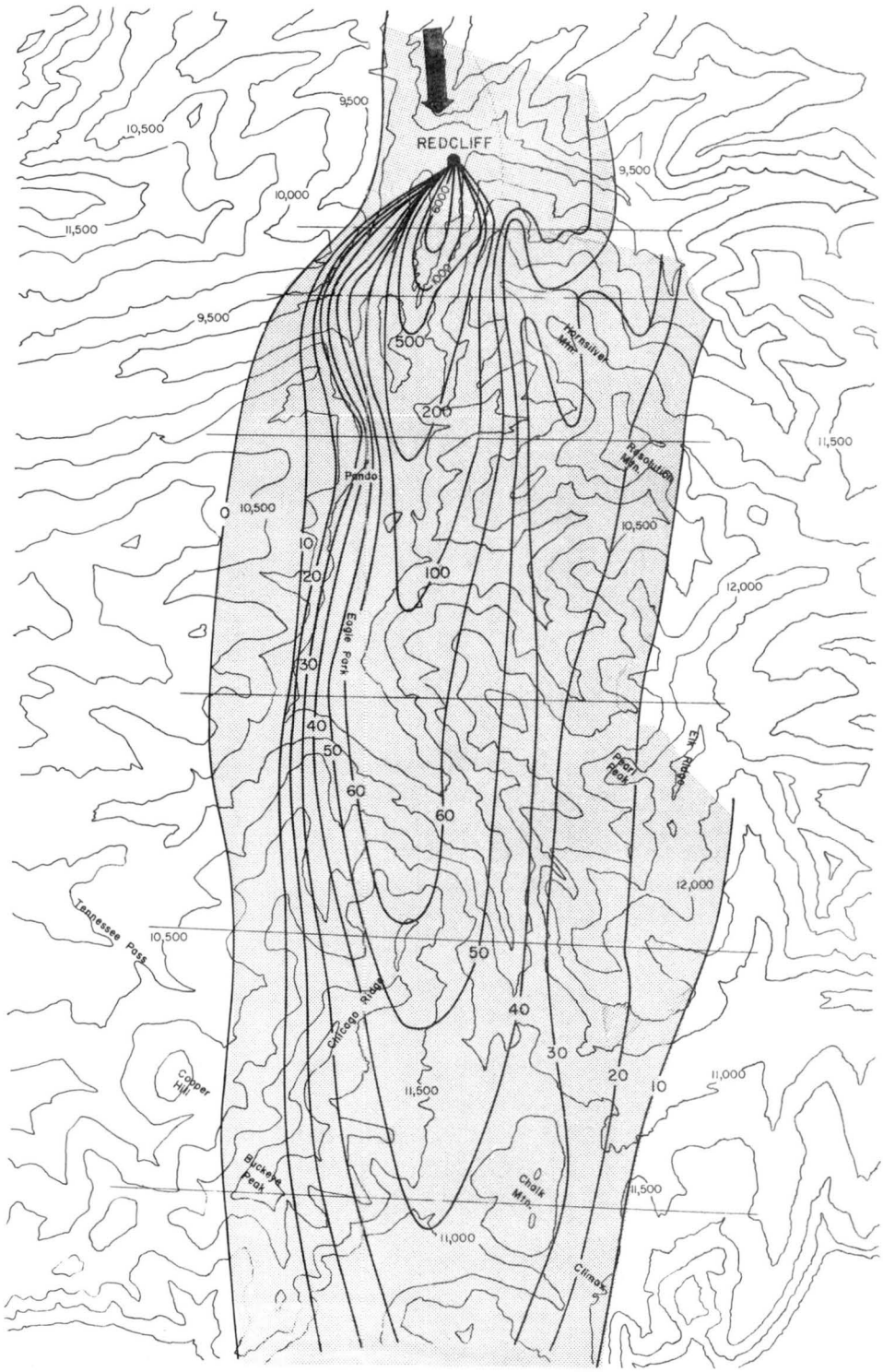

Figure 19 Surface concentration $\frac{\bar{X}\,\bar{U}}{Q} \times 10^{-9}(m^{-2})$ downwind from Minturn and Redcliff sources-Neutral stability flow.

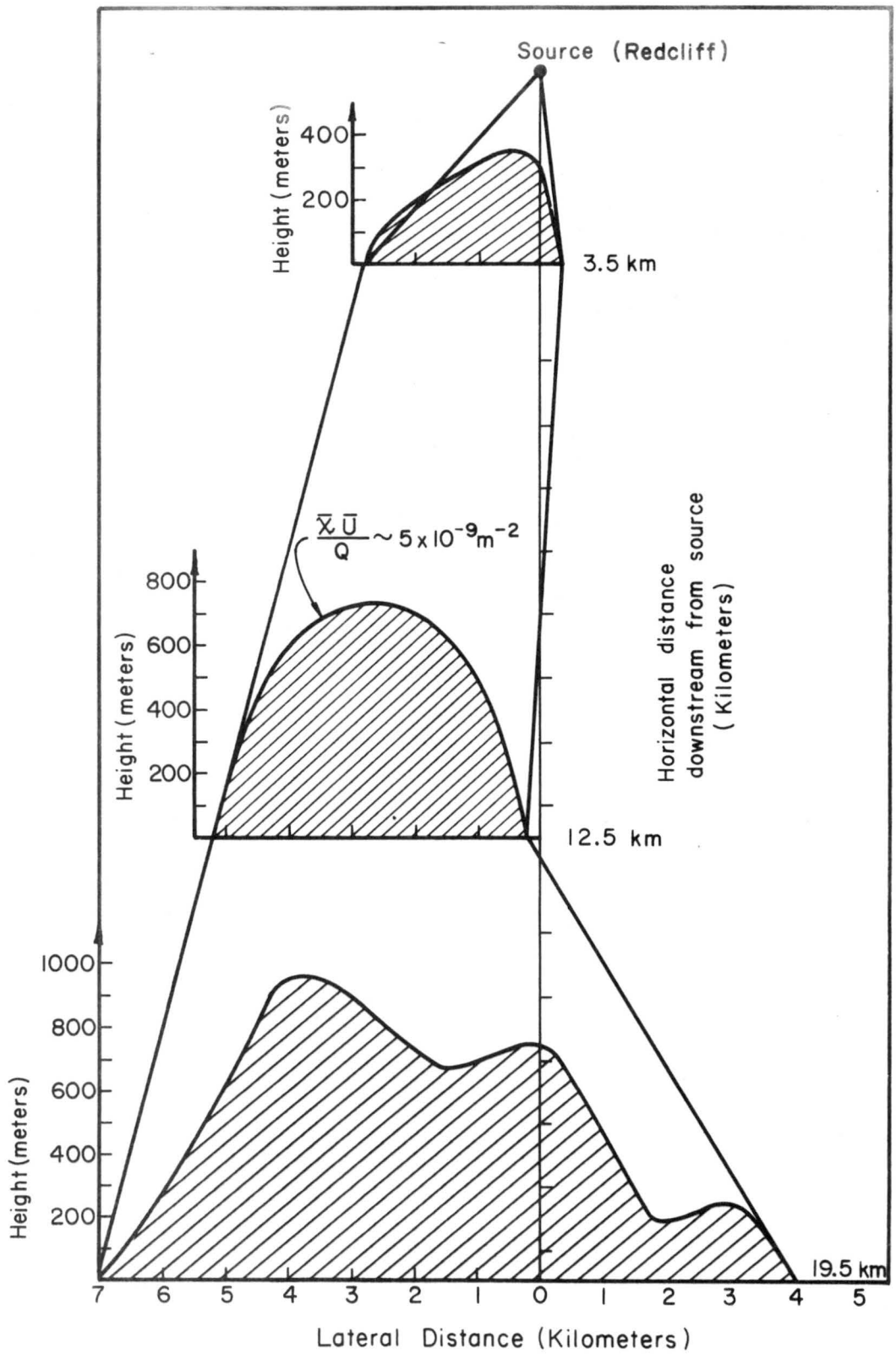

Figure 20 Cloud volume above 12,000 ft occupied by tracer material from Redcliff source-Upper boundary corresponds to $\frac{\bar{\chi}\bar{U}}{Q} = 5 \times 10^{-9} m^{-2}$.

ERRATA

p. 31 After equation (29) a paragraph was omitted. Should read -

Since no coefficients involving scaling factors enter into this equation, the only conditions necessary for similarity of the concentration field is that of geometric, thermal and dynamic similarity.

p. 56 Fig. 8 Legend should read -

Smoke-wire probe for measuring low airflow velocities.